

CLIMATE AND THE OCEAN CIRCULATION¹

I. THE ATMOSPHERIC CIRCULATION AND THE HYDROLOGY OF THE EARTH'S SURFACE

SYUKURO MANABE

Geophysical Fluid Dynamics Laboratory, ESSA, Princeton, N.J.

ABSTRACT

The effect of the hydrology of the earth's surface is incorporated into a numerical model of the general circulation of the atmosphere developed at the Geophysical Fluid Dynamics Laboratory of the Environmental Science Services Administration (ESSA). The primitive equation of motion is used for this study. The nine levels of the model are distributed so as to resolve the surface boundary layer and stratosphere. The depletion of solar radiation and the transfer of the terrestrial radiation are computed taking into consideration cloud and atmospheric absorbers such as water vapor, carbon dioxide, and ozone. The scheme treating the hydrology of our model involves the prediction of water vapor in the atmosphere and the prediction of soil moisture and snow cover. In order to represent the moisture-holding capacity of soil, the continent is assumed to be covered by boxes, which can store limited amounts of water. The ocean surface is idealized to be a completely wet surface without any heat capacity. The temperature of the earth's surface is determined in such a way that it satisfies the condition of heat balance. To facilitate the analysis and the interpretation of the results, a simple and idealized distribution of the ocean and the continental region is chosen for this study. The numerical integrations are performed for the annual mean distribution of solar insolation.

In general, the qualitative features of hydrologic and thermodynamic regimes at the earth's surface are successfully simulated. Particularly, the horizontal distribution of rainfall is in excellent qualitative agreement with the observations. For example, the typical subtropical desert, the break of the subtropical dry belt along the east coast of the continent, and the equatorial rain belt emerged as the result of numerical time integration. Some features of the spatial distributions of heat and water balance components at the earth's surface also agree well with those obtained by Budyko for the actual atmosphere.

Owing to the lack of seasonal variation of solar insolation and lack of poleward transport of heat by ocean currents in the model, excessive snow cover develops at higher latitudes. Accordingly, the temperature in the polar region is much lower than the annual mean temperature observed in the actual atmosphere.

This investigation constitutes a preliminary study preceding the numerical integration of the general circulation model of joint ocean-atmosphere interaction, in which the transport of heat by ocean currents plays an important role.

CONTENTS

1. Introduction.....	740	5. Angular momentum balance.....	750
2. Model equations.....	740	A. Surface stress.....	750
A. Equation of motion and thermodynamical equation.....	740	B. Poleward transport of angular momentum.....	750
B. Prognostic equation of water vapor.....	741	6. Hydrologic cycle.....	752
C. Radiative transfer.....	741	A. Precipitation and evaporation.....	752
D. Boundary conditions at the earth's surface.....	742	B. Runoff.....	754
E. Hydrology of land surface.....	742	C. Soil moisture.....	755
F. Distribution of ocean and continent.....	744	D. Snow budget.....	757
G. Finite differences and computational space mesh.....	744	E. Moisture transport in the atmosphere.....	757
H. Box diagram of the model structure.....	744	F. General circulation and surface hydrology.....	758
3. Time integration and the period of analysis.....	745	G. Water balance of the earth's surface.....	762
4. Time mean field.....	745	7. Heat balance.....	762
A. Temperature.....	745	A. Radiation balance of the earth-atmosphere system.....	762
B. Surface pressure.....	745	B. Poleward transport of energy.....	764
C. Zonal wind.....	746	C. Radiation balance of the earth's surface.....	765
D. Meridional circulation.....	747	D. Turbulent flux of sensible and latent heat.....	767
E. Streamlines.....	747	E. Heat balance diagram.....	768
F. Moisture.....	749	8. Eddy kinetic energy.....	768
		9. Summary and future study.....	772
		Appendix.....	773
		References.....	773

¹ In view of the length of this three-part series, it may be useful to suggest shortcuts. Readers mainly interested in the interaction between the hydrologic process and the general circulation of the atmosphere could read part I only. Readers mainly interested in the interaction between ocean and atmosphere could read sections 1 and 2 of part I and then proceed to parts II and III (Manabe, 1969, and Bryan, 1969). Those mainly interested in the general circulation of the ocean could start from part III with no difficulty.

1. INTRODUCTION

The interaction between ocean and atmosphere has received increasing attention because it plays an important role in maintaining the existing climate and in causing the long-range evolution of weather and climate. However, because of the complexity of the phenomenon, it is very difficult to determine by simple physical reasoning, or by simple analytic solution, how the ocean affects the atmospheric circulation. Therefore, it was decided to construct a mathematical model of the joint ocean-atmosphere system and to investigate the problem of ocean-atmosphere interaction by performing a series of controlled numerical experiments.

During the past several years, general circulation models of the ocean and the atmosphere have been developed separately at the Geophysical Fluid Dynamics Laboratory of ESSA. (See, for example, the studies by Bryan and Cox (1967), Smagorinsky and others (1965),² and Manabe and others (1965).³) These studies constitute the foundation for the construction of the joint ocean-atmosphere system, to be described in parts I, II, and III.

In order to facilitate the interpretation of the result, the research is carried out in three steps:

1) Study of the atmospheric model without the effect of ocean circulation. The effect of heat transfer by the ocean current is neglected. The ocean does not have any heat capacity and simply acts as an infinite reservoir of moisture for the atmosphere.

2) Study of the oceanic model without any feedback effect from the atmosphere. The distributions of surface temperature, wind stress, and precipitation over the ocean are given and assumed to be constant with respect to time.

3) Study of the joint ocean-atmosphere model in which the two systems are allowed to interact fully with each other. A comparison of the results of these three experiments sheds some light on the mutual role of the ocean in maintaining the climate and of the atmosphere in maintaining the thermal and dynamical structure of the ocean. Part I of this series of papers is limited to the description of the results obtained from the first numerical experiment, that is, the study of the atmospheric model without the effect of ocean circulation. This experiment is primarily intended to serve as a blank test, which may be compared with the later experiment including the effect of ocean circulation.

Another major objective of this study (part I) is to simulate the hydrologic cycle in the atmosphere and to find how the hydrology of the earth's surface interacts with the general circulation of the atmosphere by use of the mathematical model. In the previous study M, the earth's surface was simply assumed to be completely wet and to have no heat capacity. In this study, the amount of soil moisture and the depth of snow cover over the continent are determined through computation of the water and heat budget. The treatment of the ocean areas in part I is identical to that used for the entire earth's surface for the

previous model. To facilitate the analysis and the interpretation of the results, a simple distribution of ocean and flat continent bounded by meridians is adopted. The results from the numerical time integration of this model should be useful for studying how the moisture supply from the model ocean affects the hydrology over the continent.

2. MODEL EQUATIONS

Since the details of the system of model equations have already been described in S and M, only a brief outline of the system is given in this section.

A. EQUATION OF MOTION AND THERMODYNAMICAL EQUATION

Using the hydrostatic approximation, and pressure normalized by surface pressure as the vertical coordinate, one can write the equations of motion on the Mercator projection as

$$\frac{\partial}{\partial t} (P_* U) = -\mathcal{D}_3(U) + \left(2\Omega + \frac{mU}{a}\right) \cdot P_* V \cdot \sin \theta - mP_* \frac{\partial \phi}{\partial x} - mRT \frac{\partial P_*}{\partial x} + F_x \quad (1)$$

and

$$\frac{\partial}{\partial t} (P_* V) = -\mathcal{D}_3(V) - \left(2\Omega + \frac{mU}{a}\right) \cdot P_* U \cdot \sin \theta - mP_* \frac{\partial \phi}{\partial y} - mRT \frac{\partial P_*}{\partial y} + F_y. \quad (2)$$

The continuity equation is

$$\frac{\partial P_*}{\partial t} = -\mathcal{D}_3(1). \quad (3)$$

The hydrostatic equation is

$$\frac{\partial \phi}{\partial Q} = -\frac{RT}{Q}. \quad (4)$$

The thermodynamical equation is

$$\frac{\partial}{\partial t} (P_* T) = -\mathcal{D}_3(T) + \frac{R}{c_p} \frac{T_w}{Q} + F_T + \frac{P_* \dot{q}}{c_p}. \quad (5)$$

The vertical Q - and P -velocity are obtained by the following relations

$$\dot{Q} = \frac{1}{P_*} \left[Q \int_0^1 \mathcal{D}_2(1) dQ - \int_0^Q \mathcal{D}_2(1) dQ \right] \quad (6)$$

and

$$\omega = P_* \dot{Q} + Q \dot{P}_*. \quad (7)$$

where

$$\mathcal{D}_3(A) = \mathcal{D}_2(A) + P_* \frac{\partial(QA)}{\partial Q} \quad (8)$$

and

$$\mathcal{D}_2(A) = m^2 \left[\frac{\partial}{\partial x} \left(\frac{P_* UA}{m} \right) + \frac{\partial}{\partial y} \left(\frac{P_* VA}{m} \right) \right]. \quad (9)$$

^{2, 3} Hereafter, these papers will be referred to as S and M, respectively.

The following symbols are used:

x, y	abscissa and ordinate of Mercator rectangular coordinate (positive eastward and northward)
t	time
U, V	earth velocity components, east and north directions
P	atmospheric pressure
P_*	atmospheric pressure at the lower boundary
T	temperature
Q	P/P_*
\dot{Q}	dQ/dt
ω	dP/dt
θ	latitude
m	map scale factor for Mercator projection
q	rate of heating
$\frac{F_z}{P_*}, \frac{F_y}{P_*}$	rate of momentum change due to Reynolds stress in east and north directions
$\frac{F_T}{P_*}$	rate of temperature change due to subgrid scale diffusion of heat
R	gas constant of air
c_p	specific heat of air under constant pressure
a	radius of the earth
Ω	angular velocity of earth
ϕ	geopotential height of the constant Q -surface
K	kinetic energy

The expression of subgrid scale momentum mixing terms, F_z , F_y , and the thermal mixing term, F_T , is given in S.

B. PROGNOSTIC EQUATION OF WATER VAPOR

The change in the mixing ratio of water vapor, r , due to the advection and subgrid scale diffusion may be expressed as follows

$$\frac{\partial}{\partial t} (P_* r)_{ADV} = \mathcal{D}_3(r) + Fr \quad (10)$$

where Fr/P_* represents the change of mixing ratio due to subgrid scale diffusion. See M for the details of Fr .

If the mixing ratio of water vapor tends to exceed the saturation value of the mixing ratio resulting from the advection and the subgrid scale diffusion, convective or nonconvective condensation is assumed to take place. For a description of the details of the scheme of treating condensation and moist and dry convection, see M.

C. RADIATIVE TRANSFER

The temperature change due to radiative transfer is computed as a function of the vertical distribution of atmospheric absorbers and of temperature. The atmospheric absorbers taken into consideration are water vapor, carbon dioxide, ozone, and clouds. The details of the computation scheme have been discussed by Manabe and Strickler (1964) and Manabe and Wetherald (1967).

The solar insolation at the top of the atmosphere is assumed to be similar to the annual mean distribution. The diurnal and daily variation of solar radiation is eliminated by employing the effective mean zenith angle (Manabe and Möller, 1961). Annual mean climatological distributions of water vapor, cloudiness, carbon dioxide, and ozone are specified for the computation of radiative transfer. The distributions of tropospheric water vapor and cloudiness are identical with those used in studies S and M. The mixing ratio of water vapor in the

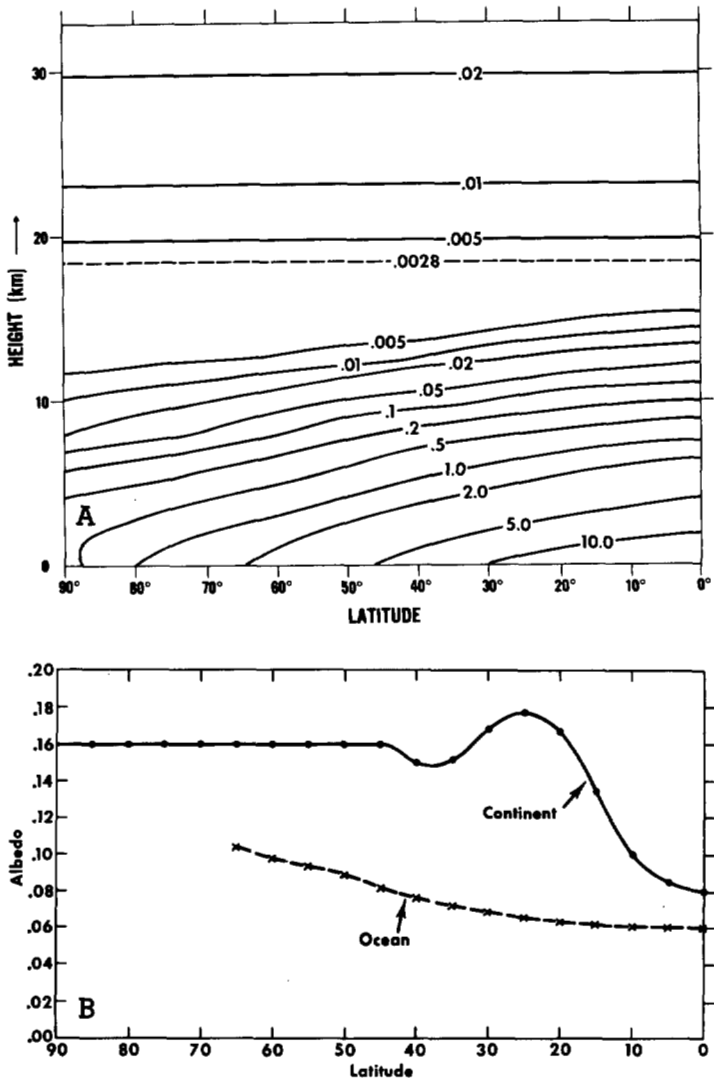


FIGURE 1.—(A) latitude-height distribution of the mixing ratio of water vapor (gm/kgm of air) used for the computation of radiative transfer; (B) latitudinal distributions of albedo chosen for this study; dashed and solid lines show the distribution for the ocean and snow-free continent, respectively.

stratosphere is assumed to be 3×10^{-6} gm/gm of air as Mastenbrook (1965) suggested. Figure 1A shows the fixed latitude-height distribution of the mixing ratio of water vapor and table 1 lists the height and the amount of cloud specified for this study. It would be possible to use the distribution of water vapor, obtained from the prognostic equation of water vapor, rather than the climatological distribution for the calculation of radiative transfer; however, to avoid a sudden increase in the degree of freedom of the model in comparison to previous studies, this is not done. In short, a part of the interaction between the hydrologic cycle and the radiation regime in the atmosphere is eliminated. The distribution of ozone is determined from the recent ozonesonde measurements by Hering and Borden (1965). Their total amounts are normalized in such a way that they coincide with the distributions compiled by London (1962) using the extensive measurements of total ozone amount obtained by the Dobson spectrometer. The annual mean distributions are obtained by taking the arithmetic average of the four

TABLE 1.—Cloud distribution adopted for this study. The height of low cloud is obtained by taking a weighted mean of the height of low cloud and that of cumuliform cloud.

Latitude	High		Middle		Low		
	Amount	Height	Amount	Height	Amount	Cloud top	Cloud base
0	0.241	9.80	0.080	4.35	0.330	3.00	1.40
5	.225	9.82	.075	4.40	.317	3.04	1.47
10	.205	10.13	.068	4.45	.290	3.08	1.61
15	.181	10.35	.064	4.50	.264	3.08	1.70
20	.168	10.50	.060	4.50	.249	3.01	1.72
25	.160	10.50	.063	4.41	.248	2.91	1.71
30	.159	10.38	.070	4.26	.269	2.80	1.70
35	.181	10.03	.079	4.10	.302	2.70	1.65
40	.192	9.44	.095	3.92	.343	2.60	1.58
45	.210	8.65	.110	3.79	.388	2.47	1.50
50	.227	7.97	.122	3.67	.417	2.35	1.40
55	.242	7.65	.131	3.56	.438	2.24	1.31
60	.250	7.29	.128	3.51	.447	2.17	1.25
65	.254	7.13	.119	3.50	.444	2.10	1.20
70	.264	7.03	.117	3.48	.439	2.03	1.12
75	.262	7.01	.111	3.44	.424	1.98	1.05
80	.231	6.99	.102	3.43	.401	1.91	1.02
85	.205	6.98	.092	3.43	.375	1.88	1.00
90	.198	6.98	.090	3.43	.360	1.87	1.00

seasons. The mixing ratio of carbon dioxide is assumed to be 0.456×10^{-3} gm/gm of air and is identical with that chosen in the studies S and M.

For the albedo and the absorptivities of clouds at various altitudes, the values used by Manabe and Strickler (1964) are adopted. The albedo of the earth's surface is determined following a suggestion by Budyko (1956). The latitudinal distributions of albedo used for this study are shown in figure 1B. Different distributions are assigned to ocean and continent separately. However, the continental distribution is not used for snow-covered surface; an albedo of 70 percent is assigned to snow-covered areas. The prognostic equation for snow cover will be described in the latter part of this section.

D. BOUNDARY CONDITIONS AT THE EARTH'S SURFACE

The surface stress $(\tau)_*$ is computed by the following formula:

$$(\tau)_* = -\rho(h) \cdot C_D(h) \cdot |\mathbf{V}(h)| \cdot \mathbf{V}(h) \quad (11)$$

where $C_D(h)$ is the drag coefficient at height h ,

$$C_D(h) = \left(k_0 / \log_e \left(\frac{h}{z_0} \right) \right)^2, \quad (12)$$

ρ is density, $\mathbf{V}(h)$ is velocity at height h , k_0 is the Karman constant, the roughness parameter Z_0 is assumed to be 1 cm, and h is chosen to be equal to the height of the lowest prognostic level. The surface stress thus computed constitutes a lower boundary condition for the computation of Reynolds stress due to vertical mixing.

Similarly, the heat flux $(vH)_*$ is given by

$$(vH)_* = c_p \cdot \rho(h) \cdot C_D(h) \cdot |\mathbf{V}(h)| \cdot [T_* - T(h)/Q(h)]^k \quad (13)$$

where T_* is the surface temperature. The flux of latent energy $(vLH)_*$ from the ocean is obtained from the

following:

$$(vLH)_* = L \cdot E \quad (14)$$

and

$$E = \rho(h) \cdot C_D(h) \cdot |\mathbf{V}(h)| \cdot (r_{ws} - r(h)) \quad (15)$$

where L is latent heat of evaporation or that of sublimation, E is the rate of evaporation, and r_{ws} is the saturation mixing ratio of water vapor, which depends upon T_* . The formula for estimating E for a land surface is given in subsection 3E. The heat flux and moisture flux at the earth's surface constitutes the lower boundary condition for the computation of vertical mixing of heat and moisture.

The temperature of the earth's surface T_* used for the computation of heat and moisture fluxes from the earth's surface is determined so that it satisfies the requirement of the heat balance at the earth's surface. If we assume that the heat capacity of the earth is zero (no heat conduction into soil), the equation of the requirement of the heat balance is

$$S_* + (DLR)_* = \sigma T_*^4 + (vH)_* + (vLH)_* \quad (16)$$

where S_* and $(DLR)_*$ are the net downward solar insolation and the downward long-wave radiation at the earth's surface, respectively, and σ is the Stefan-Boltzmann constant. Since the diurnal variation of solar insolation is eliminated in the model, it may be justifiable to neglect the heat conduction into the soil.

This scheme for computing T_* is applied to the ocean surface as well as the land surface; therefore, the downward conduction of heat into the sea is neglected. This assumption does not hold when the heat storage of the sea water changes with time or when the advection of heat by ocean currents is significant. Since we consider a model without seasonal and diurnal variation of solar insolation, the time variation of heat storage in the ocean can be neglected. On the other hand, the effect of heat advection is not negligible. Therefore, in part I we are effectively considering a hypothetical ocean or wet surface that does not transport heat horizontally.

E. HYDROLOGY OF LAND SURFACE

In this subsection, the scheme simulating the hydrology of the continent is described in detail, since it is not considered in the previous studies S and M.

Evaporation—The evaporation from a sufficiently wet land surface (including a surface covered by dense vegetation) or ocean has already been given by equations (14) and (15). Similarly, the evaporation from the surface of ice or snow, E , is

$$E = \rho(h) \cdot C_D(h) \cdot |\mathbf{V}(h)| \cdot (r_{is} - r(h)) \quad (17)$$

where r_{is} is the mixing ratio at ice saturation and $C_D(h)$ is the drag coefficient.

When the soil does not contain a sufficient amount of water, the amount of evaporation is smaller than the one obtained from equation (15). In other words, this equation gives the upper limit of evaporation from the land surface. We may call this upper limit the "evaporability" or "potential evaporation." In order to compute the evaporation from the soil which is not wet completely, it

is also necessary to take into consideration the supply of moisture from the soil as well as the turbulent transport of water vapor in the atmosphere. In the soil, moisture exists both in gas and liquid phases. The liquid moisture moves due to capillary effect, and water vapor diffuses due to molecular diffusion. The transition between water vapor and liquid water also takes place depending upon the temperature distribution in the soil. Taking into consideration these complicated processes, Philip and de Vries (1957) set up the equations for the diffusion of soil moisture as well as the conduction of heat. Their method is straightforward and seems to be suitable for the application to the limited area where the detailed characteristics of the soil are known. For our general circulation model, however, a simpler scheme is desirable because the solution of these equations requires a great amount of computation and we know little about those detailed characteristics of the various soils in the world required in their framework.

Budyko (1956) proposed a simpler scheme to obtain the amount of evaporation based upon observations of various authors. The basic principles that he adopted are as follows.

At soil moisture W , which is larger than a certain critical value W_K , total evaporation depends mainly on meteorological factors and is equal to the evaporability E_0 . When the amount of soil moisture is below W_K , evaporation becomes less than evaporability, whereupon the rate of evaporation is proportional to the amount of soil moisture.

These principles are to be summarized as follows:

$$\text{if } W \geq W_K, \quad E = E_0 \quad (18)$$

and

$$\text{if } W < W_K, \quad E = E_0 \frac{W}{W_K}$$

where

$$E_0 = \rho(h) \cdot C_D(h) \cdot |\mathbf{V}(h)| \cdot (r_{ws} - r(h)) \quad (19)$$

and W is the soil moisture contained in the soil layer from the surface to 1-m depth.

This choice of the soil layer of 1-m depth is due to the results of Romanova (1954). She found that, in the steppes and in the wooded steppe zone as well as in the forest zone, the change of moisture content in the layer of 0.5 to 1 m is quite comparable to the change in the layer of 0 to 0.5 m and is often greater. On the other hand, taking into consideration the fact that most of the root system of a plant is concentrated in the top 1-m depth, it is acceptable that most of the variation of the amount of soil moisture takes place in this layer.

Concerning the magnitude of W_K , Alpatov (1954) found that the first stage of evaporation mentioned before is observed inside a rather large range of soil moisture variations. According to him, when soil moisture is not lower than 70 or 80 percent of its field capacity, evaporation from crop field is close to the value of evaporability, that is,

$$W_K = 0.75 \times W_{fc} \quad (20)$$

where W_{fc} is the field capacity of moisture, that is, the upper limit of water that can be stored in the soil. This simple scheme was well verified by Berliand (1952) and others, and is adopted for our present purpose.

Prognostic equation of soil moisture—In order to compute the amount of evaporation by this scheme, it is necessary to know the total amount of soil moisture contained in the soil of 1-m depth. A scheme of forecasting the amount of moisture in the soil was also described by Budyko (1956). This method for the calculation of the accretion of moisture into the soil is very simple; nevertheless, it seems to catch the essential features of the phenomenon. When one combines this method with the scheme of computing evaporation described above, a scheme for the prediction of the amount of soil moisture is constructed.

According to the measurements of various authors (for example, Free and others, 1940), the infiltration rate of water into dry soil is usually faster than the rate of rainfall, except in the case of severe storms. Therefore, when there is enough available storage, the rate of accretion is almost equal to that of rainfall; other factors such as the interception by vegetation are relatively small and need not be considered. When there is no available storage, accretion is impossible, and most of the precipitated water eventually runs off by various routes.

After adopting these accretion relations verified by the authors mentioned above and after taking into consideration the effect of evaporation, the rate of the change of soil moisture can be expressed by the following equations:

$$\text{if } W = W_{fc} \text{ and } R_A > E_0, \quad \partial W / \partial t = 0 \text{ and } r_f = R_A - E_0$$

$$\text{and} \quad (21)$$

$$\text{if } W < W_{fc}, \quad \partial W / \partial t = R_A - E$$

where R_A is the rate of rainfall and r_f is that of runoff.

The field capacity of soil varies widely and depends very much upon the kind of soil (for example, the U.S. Department of Agriculture, 1955). It was decided, however, to choose a single value of 15 cm everywhere to facilitate the interpretation of the results. Palmer (1966) suggested this value based upon his experience of computing average annual runoff. This value may be somewhat smaller than the median value of field capacity, but it was chosen by Palmer because the loss of somewhat less than 100 percent of soil moisture changes the wet surface to a dry surface.

Snow cover—The equation for the prediction of the water equivalent depth of snow S is

$$\partial S / \partial t = S_f - E - M_e \quad (22)$$

where S_f is the rate of snowfall, M_e is the rate of snow melt, and E is the evaporation. M_e can be calculated using the heat balance condition of the snow-covered surface, that is,

$$M_e = E_x / L_f \text{ if } E_x > 0$$

and

$$M_e = 0 \text{ if } E_x \leq 0$$

$$(23)$$

where L_f is the latent heat of fusion and

$$E_x = [S_* + (DLR)_* - \sigma T_*^4 - (\nu H)_* - (\nu LH)_*]_{T_* = T_f} \quad (24)$$

where T_f is the temperature for freezing and is equal to 273.2°K (see equation (13) for $(\nu H)_*$ and equations (14) and (17) for $(\nu LH)_*$).

After the snow disappears through melting or sublimation, the moisture begins to evaporate from the soil surface again. Accordingly, it is also necessary to follow the amount of soil moisture even when the soil is covered by snow. In order to do this, we must know the moisture-holding capacity of snow. The water-holding capacity of snow varies depending on the density and depth; the mass of ice layers; the size, shape, and spacing of snow crystals; and the degree of channelization and honeycombing. It is difficult, if not impossible, to evaluate the individual influences of each of these factors on the liquid water-holding capacities of snow pack. The liquid water-holding capacity of snow may be related to density. Usually, the affinity of snow for liquid water increases with increasing snow-pack density. From the results of observations of thermal quality and from Gerdel's study (1954) of transmission of water through the snow, between 2 and 5 percent by weight is recommended for the liquid water-holding capacity. In this study, for the sake of simplicity, we shall assume that the moisture-holding capacity of snow is zero. After using this assumption, the forecasting of soil moisture under snow cover could be done by using the following:

$$\text{if } W < W_{fc}, \quad \partial W / \partial T = M_e + R_A$$

and

$$(25)$$

$$\text{if } W = W_{fc}, \quad \partial W / \partial t = 0 \text{ and } r_f = M_e + R_A.$$

Due to the effects of freezing, melting, and sublimation of soil moisture, the actual processes could be more complicated than those considered here.

F. DISTRIBUTION OF OCEAN AND CONTINENT

Figure 2 shows the land-sea configuration chosen for this study. In order to save computation time, the longitudinal span of the domain is assumed to be $(2\pi/3)$ radians. Both sides of the domain are bounded by the meridian and cyclic continuity is assumed from one end of the domain to the other. The longitudinal span of the land and that of the sea are equal and are assumed to be $(2\pi/6)$ radians, except for the polar region. This longitudinal span corresponds roughly to that of North and South America or the Atlantic Ocean. The distribution of land and sea in the Southern Hemisphere is symmetric to that of the Northern Hemisphere. It is hoped that the simplicity of land-sea configuration will facilitate the analysis of the results and give us insight to the relationship between the distribution of ocean and continent and to the climate on the earth's surface.

Since we adopted the Mercator projection, it was impossible to include the Pole, and it was necessary to assume an artificial free-slip insulated wall at 81.7° latitude. It is hoped that the effect of this wall, located at very high latitudes, is not serious.

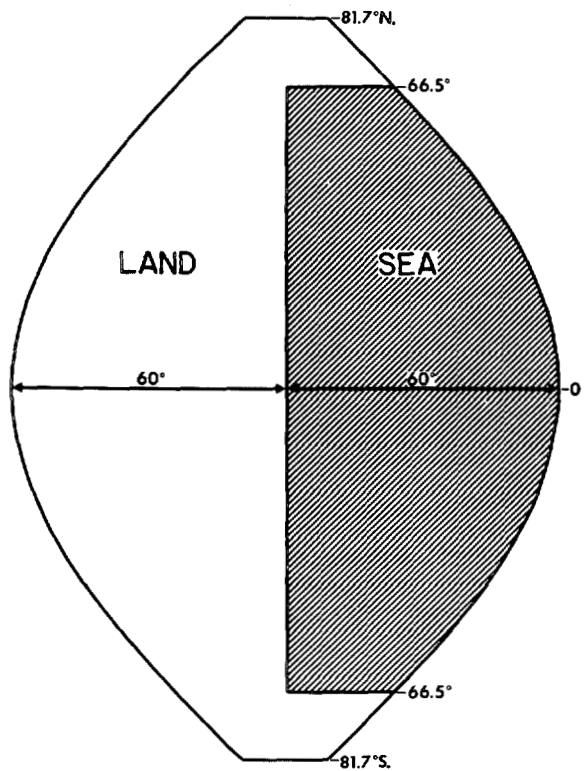


FIGURE 2.—Diagram depicting the distribution of ocean and continent. Cyclic continuity is assumed at the eastern and western ends of the domain. The distribution in the Southern Hemisphere is symmetric to the distribution in the Northern Hemisphere.

G. FINITE DIFFERENCES AND COMPUTATIONAL SPACE MESH

Arakawa (1966) proposed a finite-difference representation of the equation of motion, in which the nonlinear inertial terms are formulated to maintain some of the same integral constraints as the continuous equations and consequently avoid some of the possibilities of nonlinear instability. Based upon a similar principle, Lilly (Appendix I of study S) proposed a general energy- and momentum-conserving representation of the nonlinear term, which is adopted for this study. His formulation for the equations on the stereographic projection has already been described in S. There is no difficulty in converting his finite-difference formulation so that it corresponds to the equations on a Mercator projection, which we did for this study. Therefore, we shall not present the system of finite-difference equations here.

Figure 3 shows the distribution of computational space mesh on the Mercator projection. For example, the grid size at 45° latitude is approximately 472 km. In order to economize on the time required for the integration, the grid size on the map is doubled from 66.5° latitude and quadrupled from 71.8° . Despite the use of variable resolution, it was still possible to satisfy some of the integral constraints for the finite-difference equations by following the suggestions of Bryan (1966).

H. BOX DIAGRAM OF THE MODEL STRUCTURE

A box diagram showing the linkage among major components of the model is given in figure 4; this con-

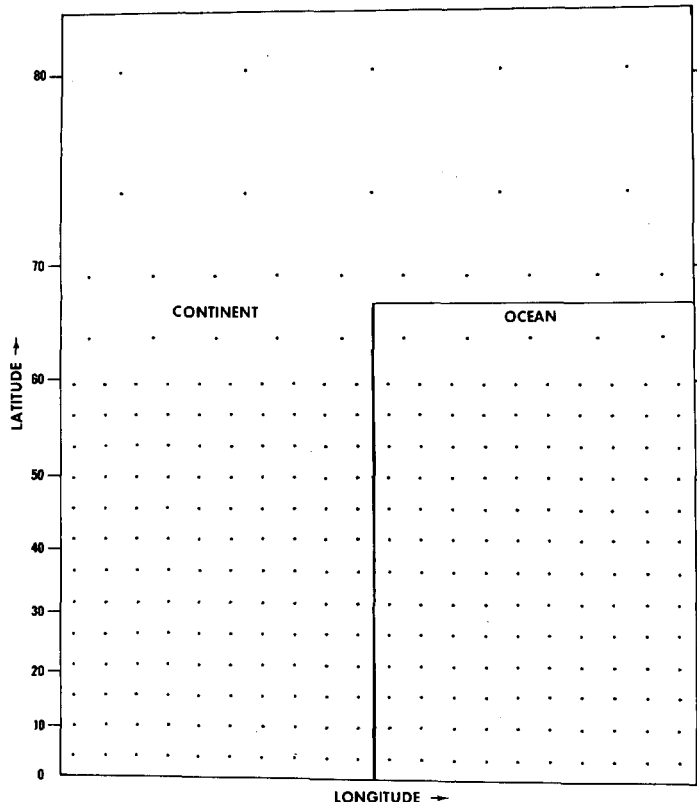


FIGURE 3.—Computational space mesh of the northern half of the domain. Grid points are indicated by dots; boundaries between ocean and continent are indicated by solid lines.

cludes the description of the model. The contents of this diagram have already been explained in the preceding subsections. The diagram is intended to give an overall view of the model structure.

3. TIME INTEGRATION AND THE PERIOD OF ANALYSIS

A quasi-equilibrium state, obtained from study M, is used as an initial condition after making it axially symmetric by taking the zonal mean. The 100-day period of the 243d to 343d model day is chosen for an analysis of the results. The quasi-steady state of the Rossby regime is reached long before this period. The results, discussed in the following sections, are obtained by taking the average of various quantities for this 100-day period except when stated otherwise.

4. TIME MEAN FIELD

Before discussing the details of the results, we shall first describe the time mean distributions of the basic quantities, that is, temperature, wind, surface pressure, and water vapor.

A. TEMPERATURE

The latitude-height distribution of the zonal mean temperature in the model atmosphere is shown in figure 5A; this may be compared with the distribution in the actual atmosphere shown in figure 5B. As in studies S and M, the general agreement between the computed and the

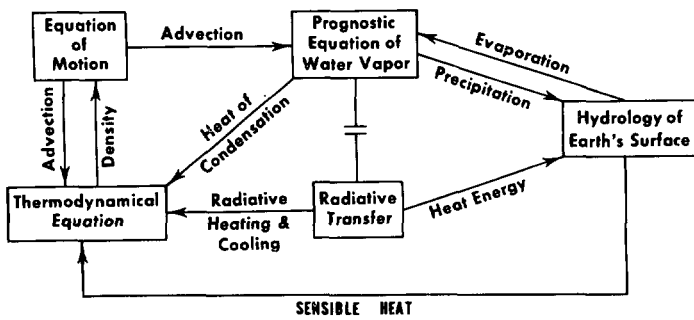


FIGURE 4.—Box diagram indicating the major components of the model. The links among the components are shown by arrows.

observed temperature distributions is excellent. There are, however, some important discrepancies. For example, figure 6, which shows the latitudinal distributions of zonal mean temperature at two isobaric levels, indicates that the temperature of the model troposphere is very low in higher latitudes. (As discussed in subsection 6D, this low temperature is mainly due to the excessive development of snow cover.) Accordingly, the latitudinal gradient of the tropospheric temperature is significantly larger in the model atmosphere than in the actual atmosphere. In part II, it will be shown that the poleward transport of heat by ocean currents helps reduce this excessive temperature gradient in the model troposphere significantly. At the stratospheric level ($P/P_* = 0.074$), the temperature of the polar stratosphere also is somewhat lower than the one obtained in M and is much lower than in the actual atmosphere. Recently, Manabe and Hunt (1968) were successful in making the temperature distribution in the model stratosphere more realistic by increasing the resolution of vertical finite differencing.

In figure 7, the horizontal distribution of temperature at the lowest prognostic level ($P/P_* = 0.991$) is compared with the horizontal distribution of temperature observed at anemometer level, obtained by taking the average between the summer (July) and winter (January) distributions. According to this figure, the temperature of the subtropical region of the continent is very high, in qualitative agreement with observation. The extremely low soil moisture and accordingly very little evaporation in this region is responsible for this high temperature. In short, a hot subtropical desert is formed in the model. This point will be discussed in more detail in sections 6 and 7. In higher latitudes, a sharp temperature contrast between ocean and continent appears. Although this feature is in qualitative agreement with observation, the surface air temperature of the continent at higher latitudes is much too low due to the excessive growth of snow cover, which has been mentioned. In the present world climate, such an extensive snow cover exists only during winter. The reason why such an extreme climate emerged in the model will be discussed in subsection 6D.

B. SURFACE PRESSURE

The latitudinal distributions of zonal mean surface pressure in the model atmosphere are contrasted with

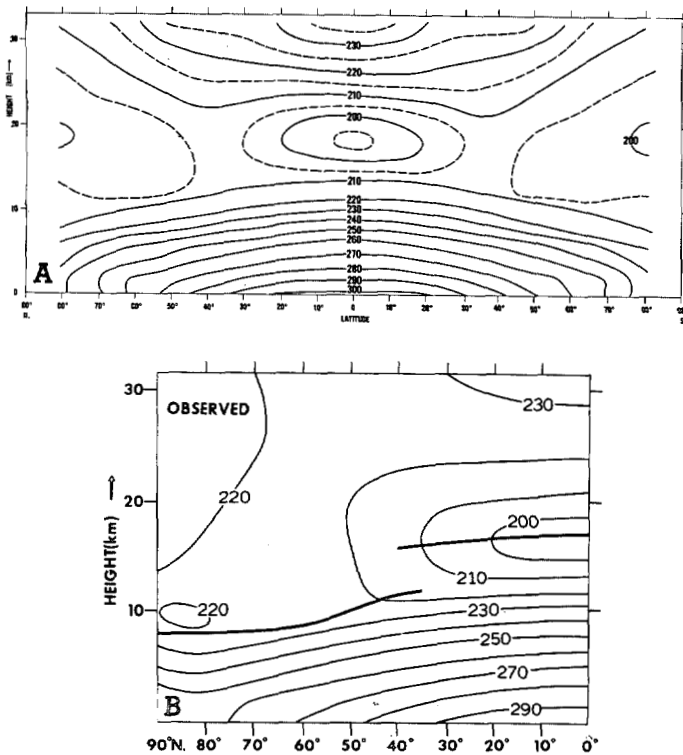


FIGURE 5.—(A) latitude-height distribution of the zonal mean temperature ($^{\circ}$ K) in the model atmosphere; (B) latitude-height distribution of the zonal mean, annual mean temperature ($^{\circ}$ K) of the actual atmosphere in the Northern Hemisphere, from the arithmetic average of the distributions of the four seasons compiled by London (1957).

those of the actual atmosphere in figure 8.⁴ The belt of low surface pressure appears in the Tropics and in middle latitudes; the belt of high pressure appears in the subtropics and in the polar region in qualitative agreement with observed features. It is rather difficult to evaluate the result quantitatively because the observed distribution is different in the two hemispheres. The surface pressure in the polar region of the model, however, seems to be excessively high. This is caused by the very cold temperature of this region (previously described).

In figure 9A, the horizontal distribution of the time mean of surface pressure is shown. For comparison, the distribution of annual mean surface pressure in the Western Hemisphere is shown in figure 9B. One of the features of interest in the numerical result is the development of an oceanic anticyclone in the model subtropics. According to the hydrostatic relationship, this anticyclone is consistent with the relatively cold air mass over the subtropical ocean. Figure 9B shows that a similar anticyclone does exist in the subtropical region of the actual Atlantic Ocean.

The opposite situation holds in the low-pressure belt in higher latitudes of the model, that is, surface pressure is somewhat lower over the ocean than over the continent. According to figure 7, the surface air temperature over the continent at higher latitudes is computed to be lower

⁴ The mean surface pressure of the model atmosphere is about 28 mb lower than the observed mean surface pressure because the model has approximately the same mass of air as the actual atmosphere but it has no mountains. For comparison, the scale (ordinate) of surface pressure of the model is shifted from that of the actual atmosphere.

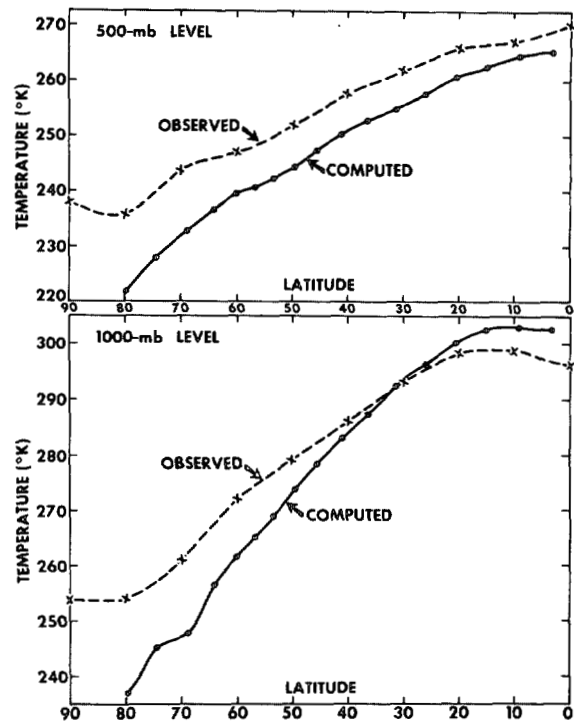


FIGURE 6.—Latitude distributions of zonal mean temperature at 500-mb and 1,000-mb levels. Solid and dashed lines indicate the computed and observed distributions, respectively. The computed distributions are obtained by taking the average of values of the two hemispheres. Observed distributions are based on the work of Peixoto (1960).

than over the ocean at comparable latitudes because the reflectivity of solar radiation by the continental snow cover is much larger than by the ocean surface. Therefore, it is reasonable to have relatively high surface pressure over the continent at higher latitudes. Also, it is well known that such heating contrast tends to enhance the development of cyclones and accordingly of the low-pressure belt over the ocean at high latitudes. For further discussion of this subject, refer to section 8.

C. ZONAL WIND

The latitude-height distribution of the zonal mean of the zonal component of wind in the model atmosphere is shown in figure 10A and can be compared with the similar distribution of zonal wind in the actual atmosphere shown in figure 10B. According to this comparison, the westerlies are generally too strong in the model atmosphere, particularly in the model stratosphere. A similar feature was evident in the model atmospheres obtained from studies S and M. Though the reason for this discrepancy is not known, it is probable that the lack of mountains in the model may be partly responsible. In the polar region of the model where the extensive snow cover and the intense anticyclone develops, the surface easterlies are significantly stronger than the actual easterlies. In the model Tropics, westerlies of significant intensity appear in the upper troposphere; whereas in the actual Tropics, easterly wind appears both in the upper troposphere and the stratosphere. Again, the reason for this discrepancy is not obvious to the author.

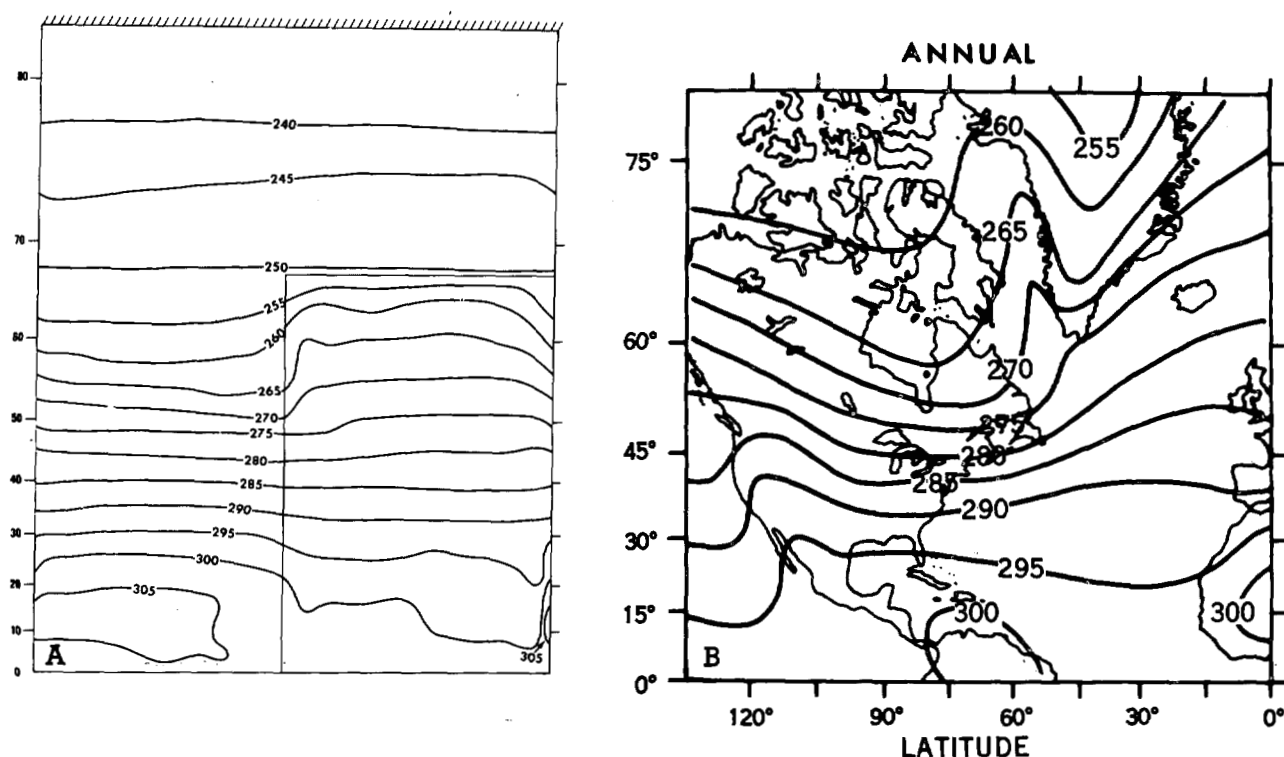


FIGURE 7.—(A) horizontal distribution of temperature ($^{\circ}$ K) at the lowest model level ($P/P_* = .991$); (B) observed distribution of temperature at sea level (Sverdrup and others, 1942); model distributions are obtained by taking the average of the two hemispheres.

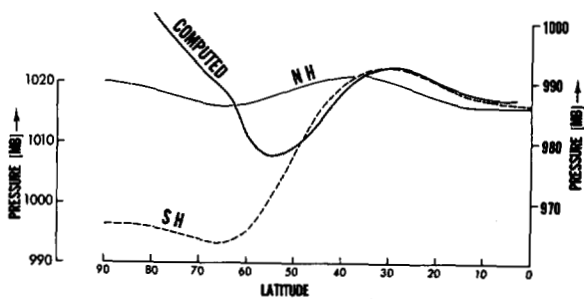


FIGURE 8.—Latitudinal distributions of the zonal mean surface pressure. The scale for the observed distributions is shown on the left ordinate and the scale for the computed distribution is shown on the right ordinate. The observed distributions for the Northern and Southern Hemispheres are indicated by NH and SH, respectively. The computed distribution is obtained by taking the average of the two hemispheres.

D. MERIDIONAL CIRCULATION

In both parts of figure 11, the latitude-height distribution of zonally averaged meridional components of the wind and of the zonally averaged vertical pressure-velocity are shown. Various features of the actual atmosphere, such as an intertropical convergence zone, a wide belt of downward motion in the subtropics, and a convergence zone in middle latitudes exist in the model atmosphere. Although the general features of the distribution are very similar to those obtained by the previous study M, there are some differences.

For example, the intensity of the direct cell in low latitudes is much stronger in the previous model M than in this model. As we shall discuss in more detail in subsection

6D, this difference is partly due to the subtropical desert, which cuts down the transfer of moisture from the subtropics into the Tropics and accordingly the intensity of the meridional circulation. (Note that in study M, the earth's surface was assumed to be wet everywhere.)

The meridional circulation patterns, obtained in studies S and M and particularly Manabe and Hunt (1968), have a very intense, localized secondary cell in the upper troposphere of the Tropics, probably due to the existence of an irregular tropical wall. Fortunately, this peculiar irregularity disappeared in the present study, which involves no tropical wall.

It is interesting that weak downward motion exists in the tropical stratosphere (at the level where $P/P_* = 0.034$). The existence of such motion in the actual atmosphere has been suggested by Tucker (1964) and Wallace (1967).

E. STREAMLINES

Horizontal distributions of the vector wind and streamlines near the earth's surface are shown in the lower half of figure 12. One of the most notable features appears in the Tropics. Air converges from the subtropics into the Tropics and forms a narrow intertropical convergence zone at the Equator. This equatorial convergence is particularly distinct in the oceanic region. Part of the converged air then moves westward onto the continent. In the subtropics, the air tends to move along the periphery of the oceanic anticyclone described in subsection 4B; simultaneously, the general divergence of air toward the Tropics and middle latitudes predominates. In middle latitudes (around 45°), southwesterly winds and in the polar region northeasterly winds prevail. Between these two regions, air

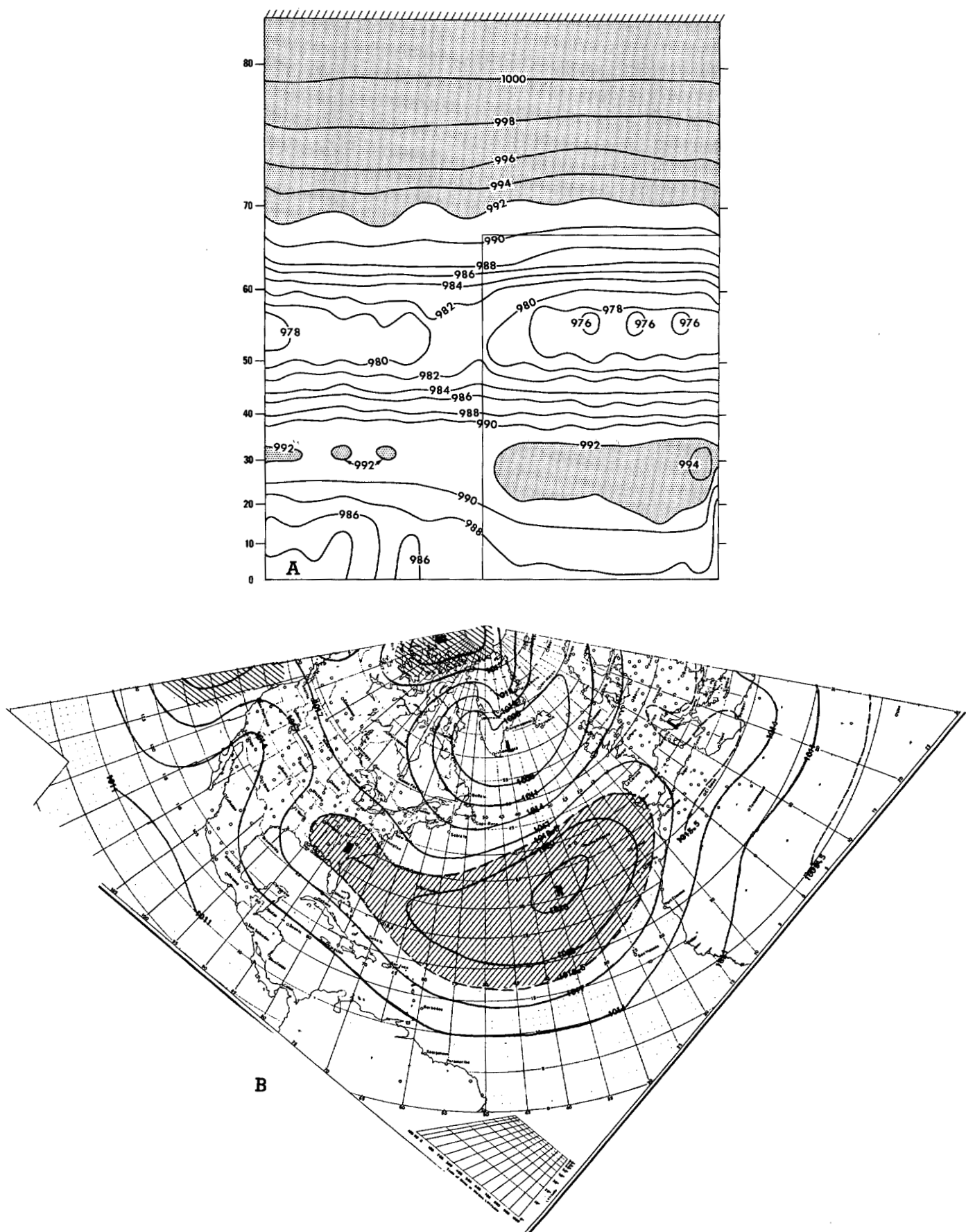


FIGURE 9.—(A) surface pressure distribution of the model (millibars), obtained by taking the average of the two hemispheres; (B) observed distribution of surface pressure (millibars) in the Western Hemisphere (annual mean distribution taken from a normal weather map published by the U.S. Weather Bureau, 1946).

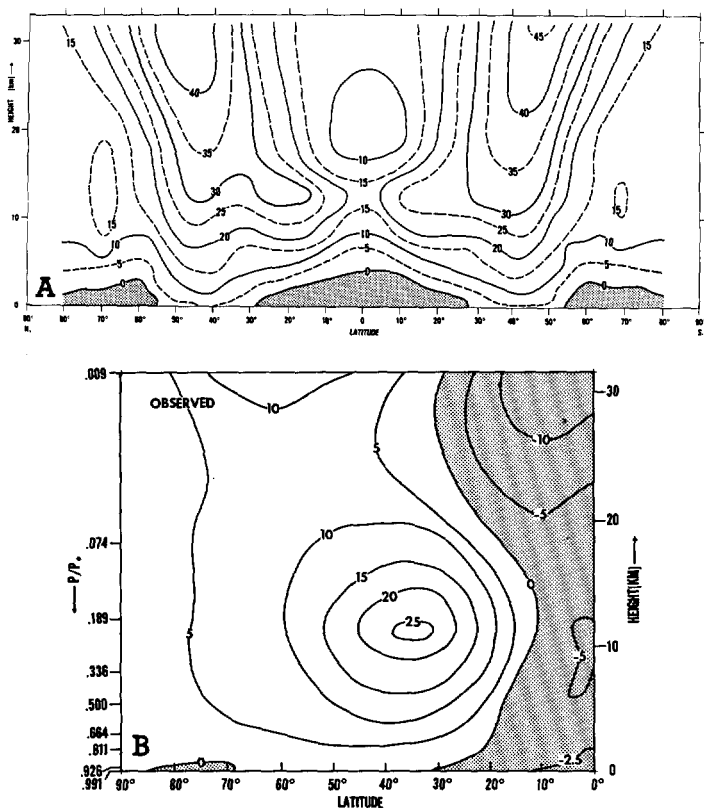


FIGURE 10.—(A) latitude-height distribution of the zonal mean of the zonal wind in the model atmosphere in units of $m \text{ sec}^{-1}$; the region of easterlies is shaded; (B) observed latitude-height distribution of the zonal mean of the zonal wind ($m \text{ sec}^{-1}$) compiled from Rasmusson and Oort (1970), Oort (1964), and Batten (1964); the region of easterlies is shaded.

converges in a zone at about 55° latitude. Similar qualitative features can be found in the wind distributions of the lower part of the actual atmosphere, which are shown in the lower part of figure 13.

Streamlines and the vector wind at about the 500-mb level ($P/P_* = 0.500$) of the model atmosphere are shown in the upper left part of figure 13. They are more or less zonal except in the oceanic region of the Tropics where air seems to diverge. In the actual atmosphere, the trough and ridgeline are evident at the 500-mb level along the east and west coasts of North America, respectively. Accordingly, the streamlines in high latitudes seem to be less zonal than those in the model atmosphere. These features of the flow in the actual midtroposphere may be due to the effect of mountains, missing in the model.

F. MOISTURE

The latitude-height distribution of the mixing ratio of water vapor in the model atmosphere is shown in figure 14. In the stratosphere, the mixing ratio is very small and increases with increasing latitude; whereas in the troposphere, it decreases with increasing latitude. Similar results were obtained in study M. The tropospheric mixing ratio in the polar region of the model is very low due to the extremely low temperature of this region.

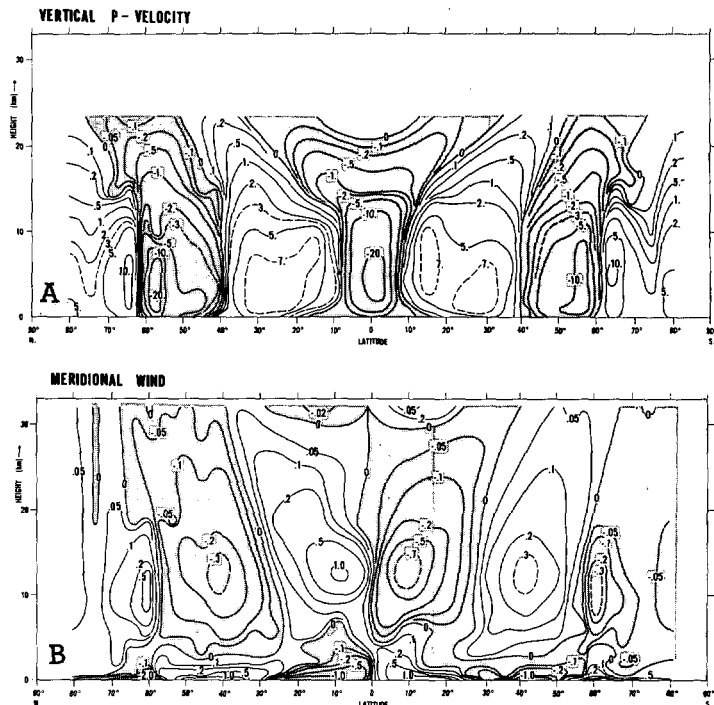


FIGURE 11.—Latitude-height distribution in the model atmosphere of (A) the zonal mean of the vertical P -velocity (mb day^{-1}) and (B) the zonal mean of the meridional component of the wind (m sec^{-1}). The regions of upward or southward components of wind are shaded.

The distribution of relative humidity in the model atmosphere is shown in figure 15A. According to this figure, the stratosphere is very dry except for the polar region where the temperature is low. It is noteworthy that a tongue of dry air penetrates into the troposphere through the region of the tropopause gap. (See Hunt and Manabe, 1968, for details of the exchange process between the model stratosphere and the model troposphere.) In general, the tropospheric relative humidity increases with decreasing altitude. Near the earth's surface, it is particularly high in the Tropics and in the higher latitudes. These features of the distribution of relative humidity in the model atmosphere are in qualitative agreement with those in the actual atmosphere. Figure 15B shows the distributions observed in the actual atmosphere during summer.

In figure 16A, the horizontal distribution of relative humidity at the lowest prognostic level is shown. One of the notable features of the results is the very dry air which covers the entire subtropical region of the continent, except for the narrow belt along the east coast. This dry region also extends slightly off the west coast of the continent. Although this dry region could correspond to the dry region located, for example, in the southwestern part of the North American Continent (fig. 16B), it seems to be too extensive. In part II, it will be shown that the ocean currents play an important role in moderating this extreme climate. Except for this desert region, the

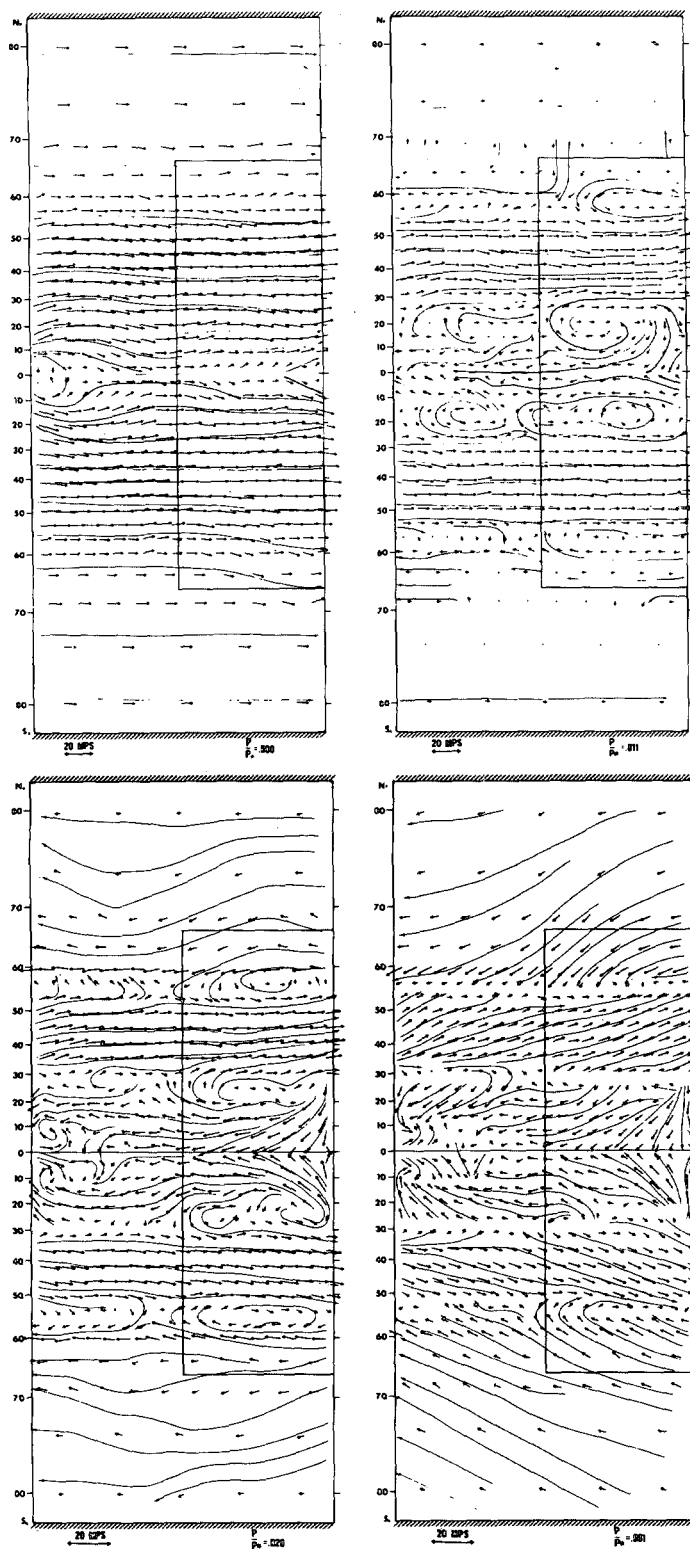


FIGURE 12.—Horizontal distributions of the vector wind at various pressure levels in the model atmosphere. The length of the 20-m sec⁻¹ vector wind is indicated near the lower left corner of each diagram. (Note that the unit length of the vector wind for the upper two diagrams is different from the unit length for the lower two.) Thin lines indicate streamlines.

level of the surface relative humidity in the model atmosphere is significantly higher than in the actual atmosphere. So far, the causes of this discrepancy have not been identified.

5. ANGULAR MOMENTUM BALANCE

The transport of angular momentum is one of the most fundamental factors controlling the general circulation of the atmosphere. Therefore, we shall describe the budget of angular momentum first.

A. SURFACE STRESS

The latitudinal distribution of surface torque of the model is shown in figure 17. Since easterlies prevail in the Tropics and polar region, the surface torque is positive, that is, the atmosphere receives angular momentum in these regions. On the other hand, the atmosphere loses positive angular momentum in the middle latitudes where westerlies reach the surface. Similar qualitative features appear in the distribution of surface torque as estimated by Priestley (1951) using observed wind, also shown in figure 17. However, there are (quantitatively speaking) various discrepancies between the two distributions. For example, the latitude of maximum negative torque of the model is located equatorward of that obtained by Priestley. Also, the magnitude of this negative torque in middle latitudes and of positive torque in the polar region seems to be too large. Because of the large albedo of the extensive snow cover in high latitudes, a large dome of cold air, and accordingly an extensive anticyclone, and the belt of the easterlies develop in the polar region as discussed in subsection 4B. This intense anticyclone and the large meridional temperature gradient in the surrounding area may be responsible for the discrepancies mentioned above.

B. POLEWARD TRANSPORT OF ANGULAR MOMENTUM

In figure 18, the latitudinal distributions of the poleward transport of angular momentum by transient eddies, standing eddies, and standing meridional circulation in the model atmosphere are compared with those in the actual atmosphere estimated by Buch (1954). The mathematical definitions of the poleward transports of any quantity q across a latitude circle by various processes are:

poleward transport of q by transient eddies

$$= (2 \cdot \pi \cdot a \cdot \cos \theta/g) \cdot \int_0^{P_{max}} (\bar{v} - \bar{v}^t) \cdot (q - \bar{q}^t) dp,$$

poleward transport of q by standing eddies

$$= (2 \cdot \pi \cdot a \cdot \cos \theta/g) \cdot \int_0^{P_{max}} (\bar{v}^t - \bar{\bar{v}}^t) \cdot (\bar{q}^t - \bar{\bar{q}}^t) dp,$$

and

poleward transport of q by standing meridional circulation

$$= (2 \cdot \pi \cdot a \cdot \cos \theta/g) \cdot \int_0^{P_{max}} \bar{v}^t \cdot \bar{q}^t dp$$

where P_{max} is maximum surface pressure and v is the meridional component of the wind. $(\overline{\quad})^t$ and $(\overline{\quad})^s$ denote the time mean and zonal mean, respectively. As figure 2 indicates, the longitudinal span of the domain of computation is $(2\pi/3)$ radians. However, the transports

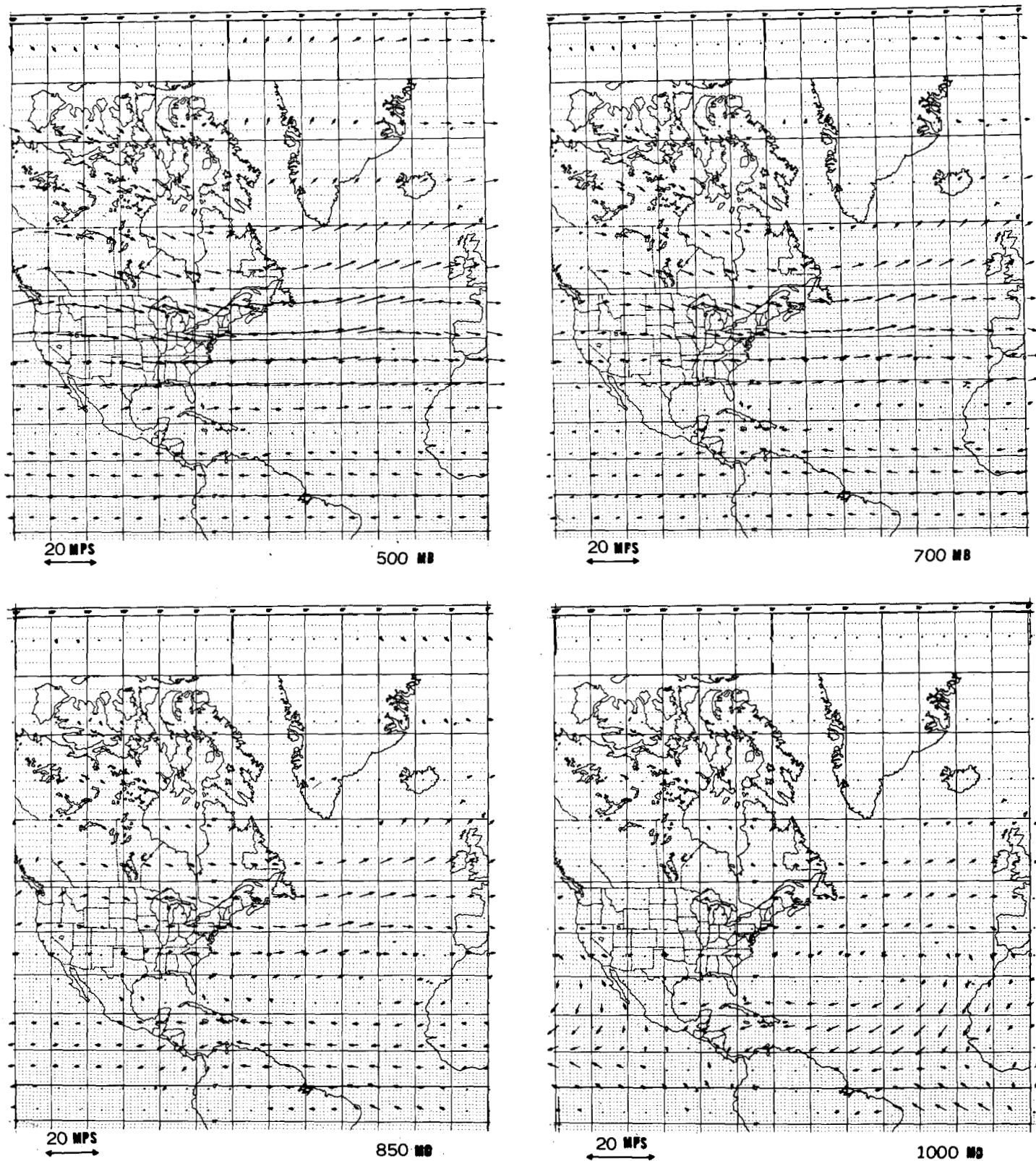


FIGURE 13.—Horizontal distributions of the vector wind at various pressure levels in the actual atmosphere. The length of the 20-m sec⁻¹ vector wind is indicated near the lower left corner of each map. (Note that the unit length of the vector wind for the 1,000-mb-level map is different from the unit length of the other three maps.) These distributions were obtained by taking the average of a 5-yr period starting from May 1958 (Rasmusson and Oort, 1970).

are defined by assuming that there are three identical domains which cover 2π radians. This assumption enables us to compare quantitatively the transports in the model atmosphere with those in the actual atmosphere.

In the subtropics, the poleward transport of angular momentum by transient eddies is a maximum and is somewhat larger than the estimate of Buch (1954). However, the magnitude of total eddy transport, which

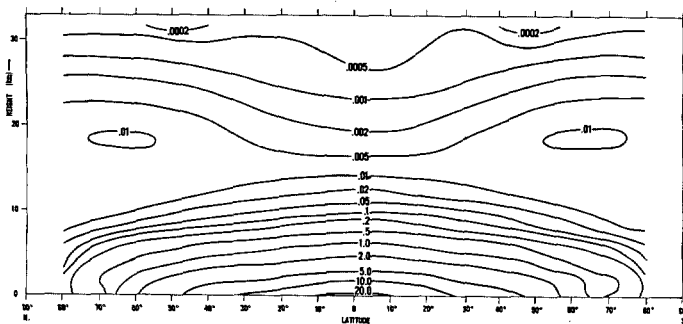


FIGURE 14.—Latitude-height distribution of the zonal mean mixing ratio of water vapor in the model atmosphere (units, gm/kgm of air).

is the sum of the contribution of transient eddies and of standing eddies, agrees reasonably well with the estimates of Buch.

In higher latitudes of the model, the large equatorial transport of angular momentum by transient eddies prevails; whereas, it is missing in Buch's distribution. As previously discussed, the anticyclone and surface easterlies prevail in the polar region due to the effect of extensive snow cover. The large supply of positive torque due to the surface easterlies is responsible for this equatorial transport of angular momentum. During the ice age, such equatorial transport probably predominated.

Figure 18 also indicates that the latitudinal distribution of the transport by standing eddies in the model atmosphere is quite different from the distribution estimated by Buch for the actual atmosphere. In view of the highly idealized orography chosen for this study, disagreement may be expected.

The distribution of the transport of absolute angular momentum by the meridional circulation in the model atmosphere also has very little similarity with the distribution obtained by Buch. Since the speed of the meridional circulation is very small, it is extremely difficult to estimate its contribution to the transport of absolute angular momentum. Therefore, it is highly probable that the distribution in the model atmosphere is more realistic than the distribution estimated by Buch.

The latitude-height distribution of angular momentum transport by transient eddies is given in figure 19. Again, relatively large equatorward transport in higher latitudes is a characteristic feature of this distribution. Another feature of interest is the equatorward transport in the upper troposphere of the Tropics. It is not certain whether such equatorward transport of angular momentum does or does not exist in the actual atmosphere.

6. HYDROLOGIC CYCLE

As we explained in the introduction, the hydrology of the earth's surface is the new feature of the model. Therefore, we shall describe and discuss the hydrologic cycle of this model in special detail.

A. PRECIPITATION AND EVAPORATION

Horizontal distributions—The distribution of precipitation (sum of rainfall and snowfall) for the model is shown

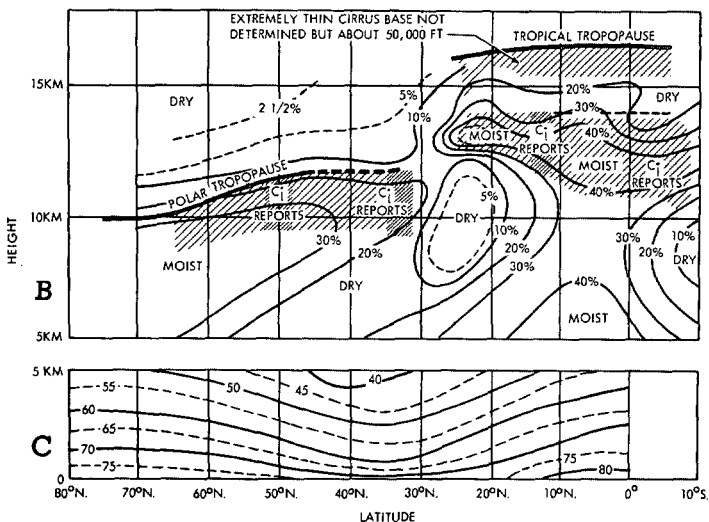
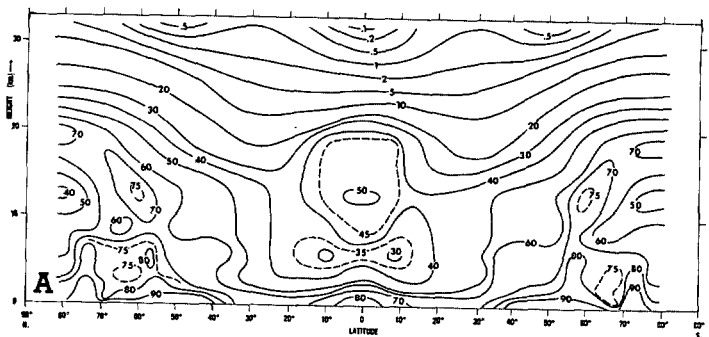


FIGURE 15.—(A) latitude-height distribution of zonal mean relative humidity in the model atmosphere (units, percent); (B) and (C) latitude-height distribution of mean relative humidities and cirrus distribution in the actual atmosphere (Northern Hemisphere) during the summer season; (B) from Murgatroyd (1960) and (C) from Telegadas and London (1954).

in the left diagram of figure 20. One of the interesting features of this distribution is the belt of intense rainfall directly at the Equator. Although the actual intertropical rain belt is not always situated at the Equator, this result suggests that it would be there if there were no asymmetries between the hemispheres, no seasonal variation, and no effect from ocean circulation. In order to establish this point firmly, it seems to be necessary to repeat this study using the model with higher resolution in the Tropics. As Manabe and Smagorinsky (1967) pointed out, the rainfall in the model Tropics results mainly from the intense vertical motion and moist convection in the synoptic scale disturbances. Thus, the distribution of the instantaneous rate of rainfall is highly variable with respect to time and space. The organized tropical rain belt in figure 20 is obtained by computing the average rate of rainfall for a period of 100 days.

In the subtropics of the model, where the downward branch of direct Hadley cell prevails, the rate of rainfall is generally very small. The area of low precipitation rate has wider latitudinal spread on the continent than on the ocean due to the self-amplification effect involved in the desert formation process to be discussed. This subtropical belt of meager rainfall is interrupted by the area of ample rain along the east coast of the continent. Similar features

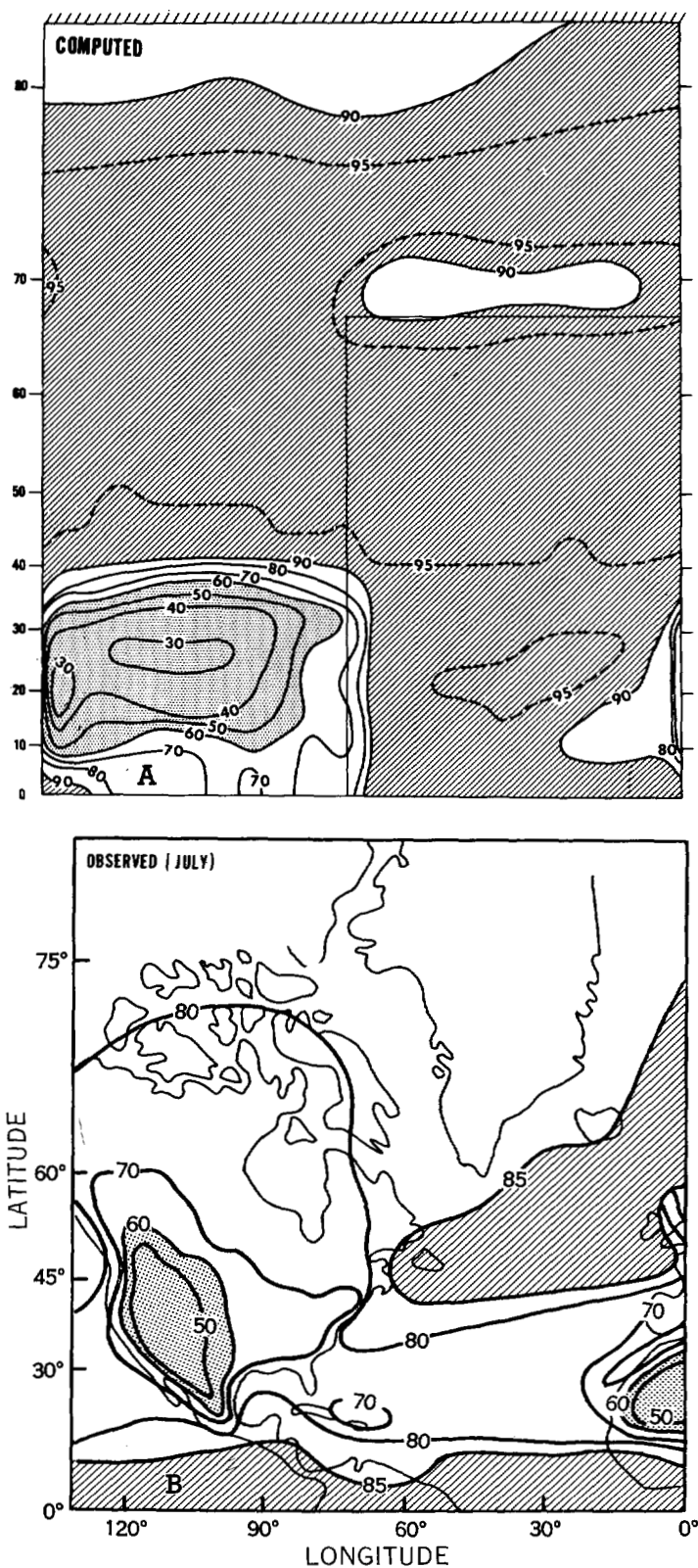


FIGURE 16.—(A) horizontal distribution of relative humidity at the lowest model level ($P/P_* = .991$) in percent; values of the two hemispheres are averaged; (B) horizontal distribution of relative humidity observed at the earth's surface (Szava-Kovats, 1938); the distribution for the month of July is shown in percent.

of rainfall can be observed along the east coasts of North America and Eurasia. (See fig. 21 for the observed distribution.)

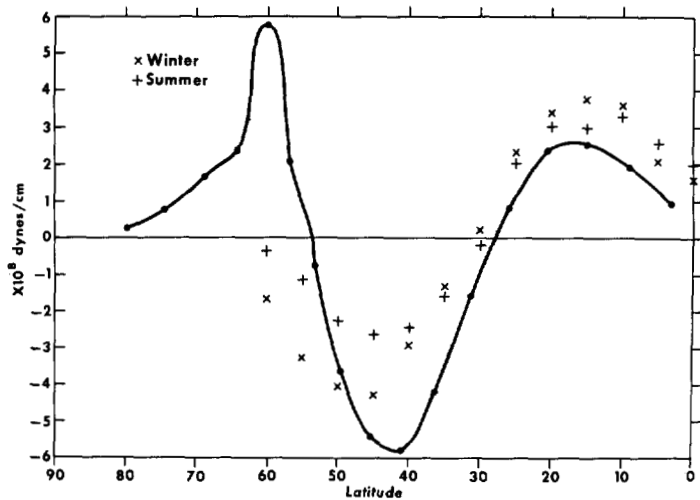


FIGURE 17.—Latitudinal distribution of surface torque of the model atmosphere. The values of surface torque in the actual atmosphere, estimated by Priestley (1951), are added by x's for winter and +'s for summer. The values of the two hemispheres are averaged.

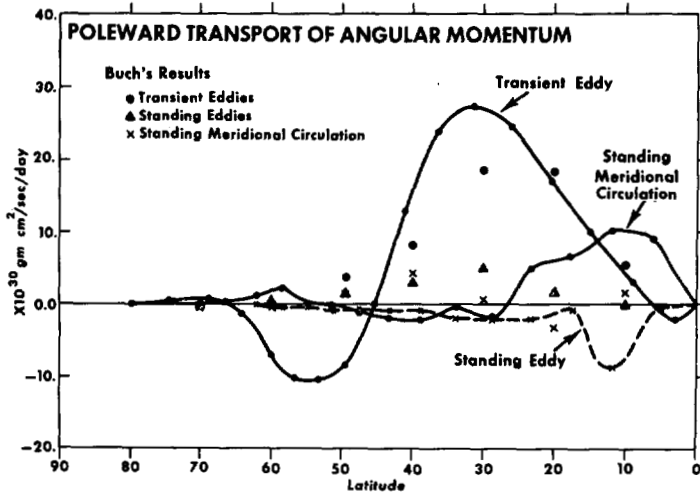


FIGURE 18.—Poleward transport of angular momentum in the model atmosphere by transient eddies, standing eddies, and standing meridional circulation, respectively. The values of the two hemispheres are averaged. The results obtained by Buch (1954) for the actual atmosphere are plotted for comparison.

The belt of relatively large precipitation rate occupies middle latitudes. In this belt, the precipitation rate is somewhat larger in the ocean than in the continent. This oceanic area of large rainfall is connected with the tropical rain belt by the rainy area of the subtropics along the east coast of the continent. These features are in qualitative agreement with the observed features. The area of intense rainfall off the west coast of the continent, however, is located too far south. According to figure 21, the area of intense rainfall should be located around 55° latitude; whereas, it is located at about 45° in the model. The results in part II indicate this discrepancy is partly due to the lack of horizontal transport of heat by ocean currents.

As one would expect, the rate of precipitation is very small in the polar region partly because of the small water

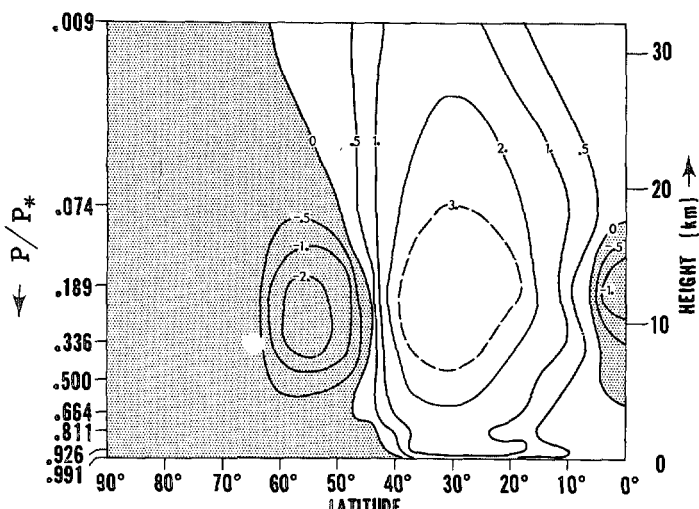


FIGURE 19.—Latitude-height distribution of poleward transport of angular momentum by transient eddies in the model atmosphere (units, $10^{28} \text{ gm cm}^2 \text{ sec mb}^{-1} \text{ day}^{-1}$). The values of the two hemispheres are averaged.

vapor content of the air. The excessive development of snow cover intensifies the dome of cold air in the polar region and is responsible for the extremely low rate of precipitation there.

The distribution of evaporation obtained from the model is given in the right diagram of figure 20.

In the land area, the rate of evaporation is a maximum in the equatorial region and very small in the subtropics where a desert develops because of the meager precipitation. In the polar region, sublimation is extremely small due to the large albedo of snow cover and to the weak solar radiation reaching the surface.

In the ocean area, the area of large evaporation extends from the Tropics to the subtropics. Around 60° latitude, the evaporation rate is significantly larger than the rate of the corresponding latitude of land area, because of the difference in surface albedo (land area is snow covered in this latitude belt).

These features are in qualitative agreement with the features of the annual mean distribution of evaporation as calculated by Budyko (1963) and shown in figure 22, but there are some discrepancies. For example, the model distribution misses the region of rapid evaporation off the east coast of the continent in the middle latitudes. This is probably because the ocean surface is not warm enough due to the lack of advection of heat by ocean currents.

Zonal mean distribution—Having discussed the area distribution of precipitation and evaporation, we shall next describe the latitudinal distribution of the zonal mean value of these quantities shown in figure 23. In the left-hand side of the figure, the computed distributions are given; and in the right-hand side, the observed distributions compiled by Budyko (1963) are added for comparison. We shall describe the distribution in three parts, that is, the oceanic region, the continental region, and the combined land and sea area.

In the oceanic region of the model, the rate of precipitation exceeds that of evaporation in the tropical and

middle latitudes; whereas, the former is much less than the latter in the subtropics. In the polar region, both rates are very small. These features agree very well with the observed features.

In the continental region of the model, the rate of evaporation is almost similar to that of precipitation, except in middle latitudes where the latter significantly exceeds the former. This middle-latitude maximum of precipitation is not observed in the continental region of the Northern Hemisphere; it is, however, observed in the Southern Hemisphere where the size of the continent is small. In the Tropics, the rate of precipitation slightly exceeds the rate of evaporation. According to the estimate of actual evaporation shown in the right-hand part of figure 23, the rate of rainfall in the tropical region of the continent far exceeds the rate of evaporation. As we shall demonstrate in part II, this discrepancy can be attributed to the lack of ocean circulation in the model.

After taking the average of the distributions of the continental region and the oceanic region, the computed distribution agrees well with the observed distribution even from a quantitative aspect. According to study M, the intensity of tropical rainfall, obtained from the numerical integration of the general circulation model, is unrealistically large and exceeds considerably the intensity of evaporation. The reason why the present study yields less rainfall in the Tropics is mainly due to the existence of land which cuts down some of the supply of moisture from the subtropics into the Tropics. In study M, the earth's surface was assumed to be completely wet.

B. RUNOFF

The distribution of the difference between the precipitation and evaporation or $(P-E)$ is shown in figure 24. In the positive area, for example, precipitation exceeds evaporation; and water is available for either runoff or the dilution of sea water.

On the continent, regions of positive $(P-E)$ appear in middle latitudes and in the Tropics. The positive region in middle latitudes is relatively wide and is responsible for large runoff in this region.

In the oceanic region, an area of large negative $(P-E)$ occupies the subtropics; and one of large positive values exists in the intertropical convergence zone. A positive area also covers middle latitudes. The net effect of this oceanic distribution is to supply water vapor to the atmosphere and accordingly to increase the salinity of sea water in the subtropics, and to remove the moisture from the atmosphere as well as to dilute the salinity in both the Tropics and middle latitudes. The coupling between hydrologic cycle and the salt balance of the ocean will be treated in the next study of the joint ocean-atmosphere model.

Figure 25 gives the latitudinal distributions of the zonal mean value of $(P-E)$ as well as that of runoff for the continental region. The difference between these two curves is mainly due to the change in soil moisture during the period for analysis. According to this figure, runoff predominates in the middle latitudes and in the Tropics.

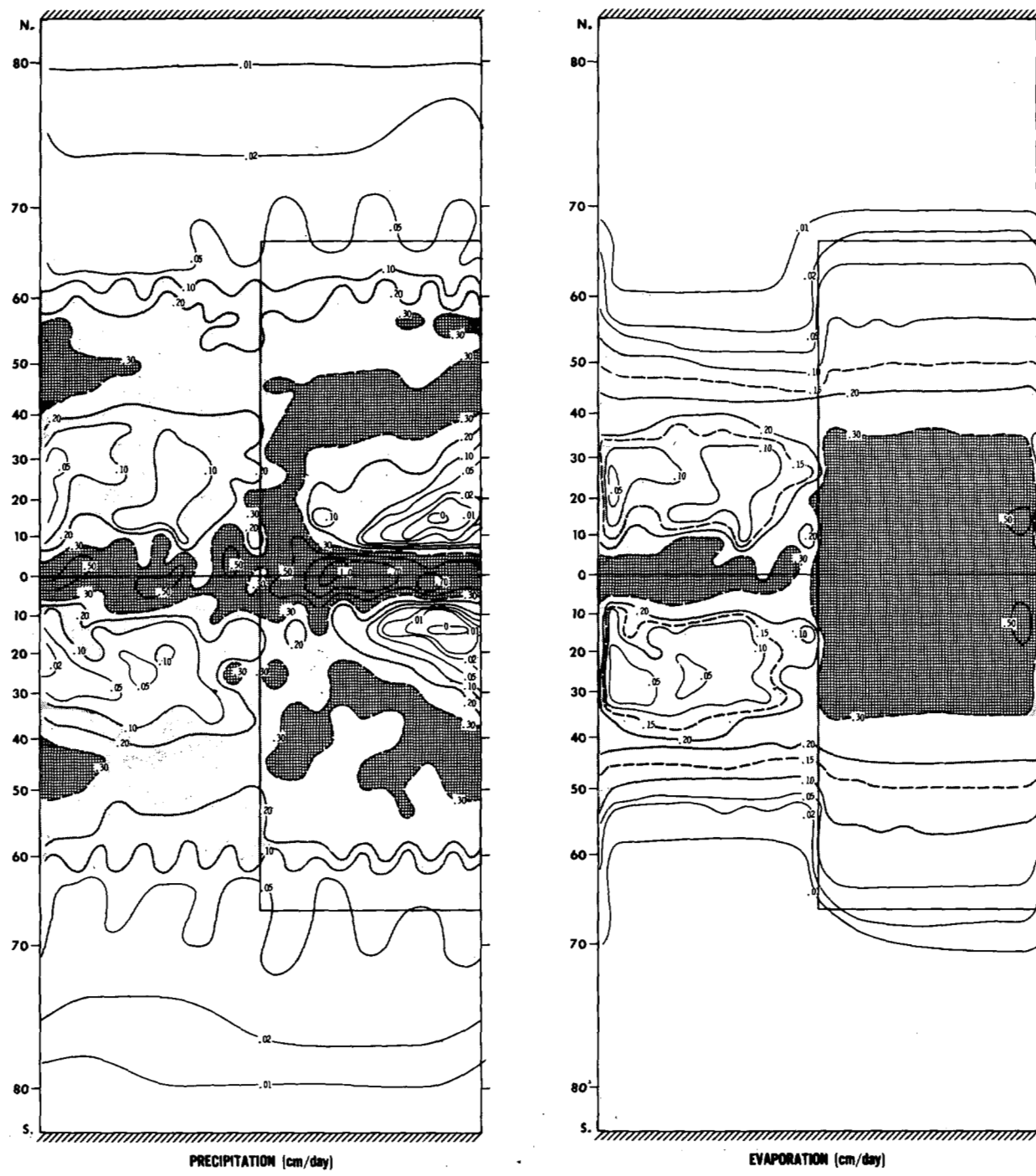


FIGURE 20.—Horizontal distribution of precipitation and evaporation of the model.

In the same figure, the estimate of runoff obtained by Lvovitch and Ovtchinnikov (1964) for both hemispheres is plotted for comparison. According to this figure, the runoff in the actual Tropics seems to be much larger than the runoff in the model Tropics. We shall discuss the causes of this discrepancy in part II. Another maximum in the rate of runoff appears in the middle latitudes of the model; whereas, the estimate of actual runoff has such a maximum only in the Southern Hemisphere. It is probable that the wide longitudinal span of the Eurasian Continent reduced the intensity of rainfall in the middle

latitude of the Northern Hemisphere and is responsible for the lack of maximum runoff there.

C. SOIL MOISTURE

The distribution of soil moisture of the model is shown in figure 26. In the subtropical region of the continent, the soil moisture is very small, that is, the subtropical desert is formed in the model as a result of extremely meager rainfall. Soil moisture increases from the subtropical desert toward the Equator and toward the east coast of the continent where the rate of rainfall is larger.

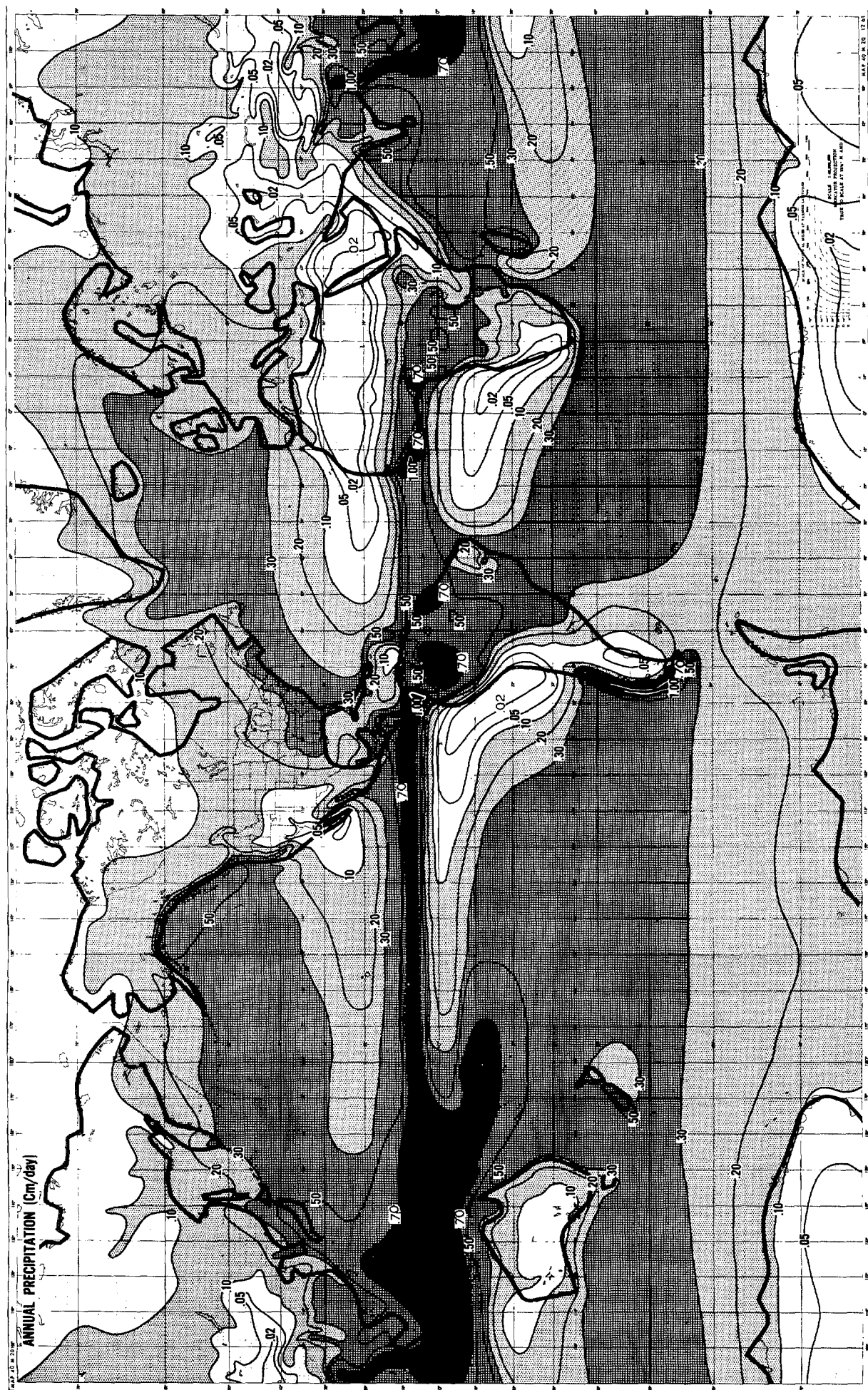


FIGURE 21.—Distribution of precipitation compiled by Lvovitch and Ovtchinnikov (1964).

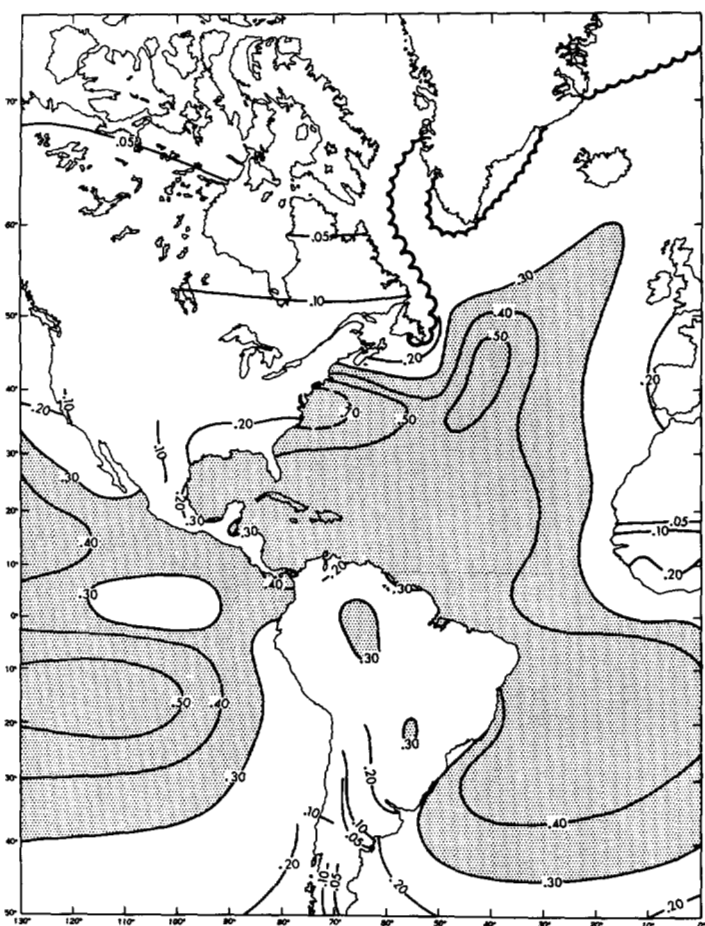


FIGURE 22.—Distribution of evaporation (cm day^{-1}) obtained by Budyko (1963).

In higher latitudes, the soil moisture is equal to the field capacity of the soil. In other words, the soil is saturated with water. This somewhat unrealistic result is probably caused by the lack of seasonal variation in the model. In high latitudes, the surface of the model earth is permanently covered by snow, which reflects most of the solar radiation reaching the surface and minimizes the rate of sublimation. (See subsection 6D.) Therefore, soil moisture hardly evaporates. Over the actual earth's surface, some of the snow cover disappears during the warm season. Thus, the soil could be dry even though the annual mean rate of precipitation exceeds that of evaporation due to the seasonal variation of the difference between precipitation and evaporation.

D. SNOW BUDGET

Figure 27 shows the latitudinal distribution of snow budget. In this figure, net accumulation of snow takes place as far south as 53° latitude. Because of the rapid snow melt south of this latitude, snow does not accumulate. Just north of this latitude, snow accumulates rather rapidly because of the large rate of snowfall and the slow sublimation rate. The extensive snow cover resulting from this snow accumulation effectively produces a cold climate which may correspond to the ice age. There are various factors that may be responsible for this cold climate. The following are some of them.

Lack of seasonal variation—During summer, snow cover would normally melt completely and would reduce the albedo drastically; therefore, the annual mean albedo could be significantly less than the albedo of a snow-covered surface even though the annual mean temperature is below freezing.

During the cold season, the net cooling at the ocean surface penetrates into the deeper layer of the ocean due to the effect of free convection; whereas during the warm season, the heating is limited to the shallow layer due to the stable stratification. Preliminary results from the integration of the model with seasonal variation indicate this difference results in the net rise of annual mean temperature of the ocean surface in higher latitudes.

Self-amplification effect of snow cover upon air temperature—The snow cover has an interesting self-amplification effect because of its large albedo. When the snow cover is more extensive, the air temperature is colder; and when the air temperature is colder, the snow cover is wider. Therefore, it is possible that a small bias in the model could easily result in an ice age. This should be an important subject for further research.

Lack of poleward transport of heat by ocean currents—This effect will be discussed in part II.

E. MOISTURE TRANSPORT IN THE ATMOSPHERE

Poleward transport—In figure 23, the atmosphere gains moisture in the subtropics and loses it in the Tropics and middle latitudes. In order to compensate for this gain and loss, atmospheric motion transports moisture. In figure 28, the poleward transport of moisture by transient or standing eddies in the model atmosphere is compared with the poleward transport in the actual atmosphere. The observed distributions were obtained from Peixoto and Crisci (1965). The distribution of poleward transport in the model atmosphere has the following features:

1) In general, the transient eddies transport moisture poleward. The maximum transport takes place between 30° and 40° latitude.

2) The meridional circulation transports large amounts of water vapor from the subtropics into the Tropics. The direct tropical cell of the meridional circulation is responsible for this. Weak poleward transport due to the indirect cell appears in middle latitudes (fig. 11).

3) Transport due to subgrid scale diffusion is very small.

4) The net effect of these transports is to remove the water vapor from the subtropics into the Tropics and the middle latitudes, thus compensating for the imbalance between evaporation and precipitation. The general qualitative features of these transports agree very well with the features of the actual atmosphere (fig. 28B).

The latitude-height distribution of the poleward transport of water vapor by transient eddies is shown in figure 29. It is interesting that equatorward transport prevails in the stratosphere. A similar result was obtained in study M. Refer to study M for a discussion of the water balance in the model stratosphere, which is very dry.

Moisture transport vector—Figure 30 was drawn in order to find how moisture is transported from the source region to the sink. The vectors indicating the vertical integral

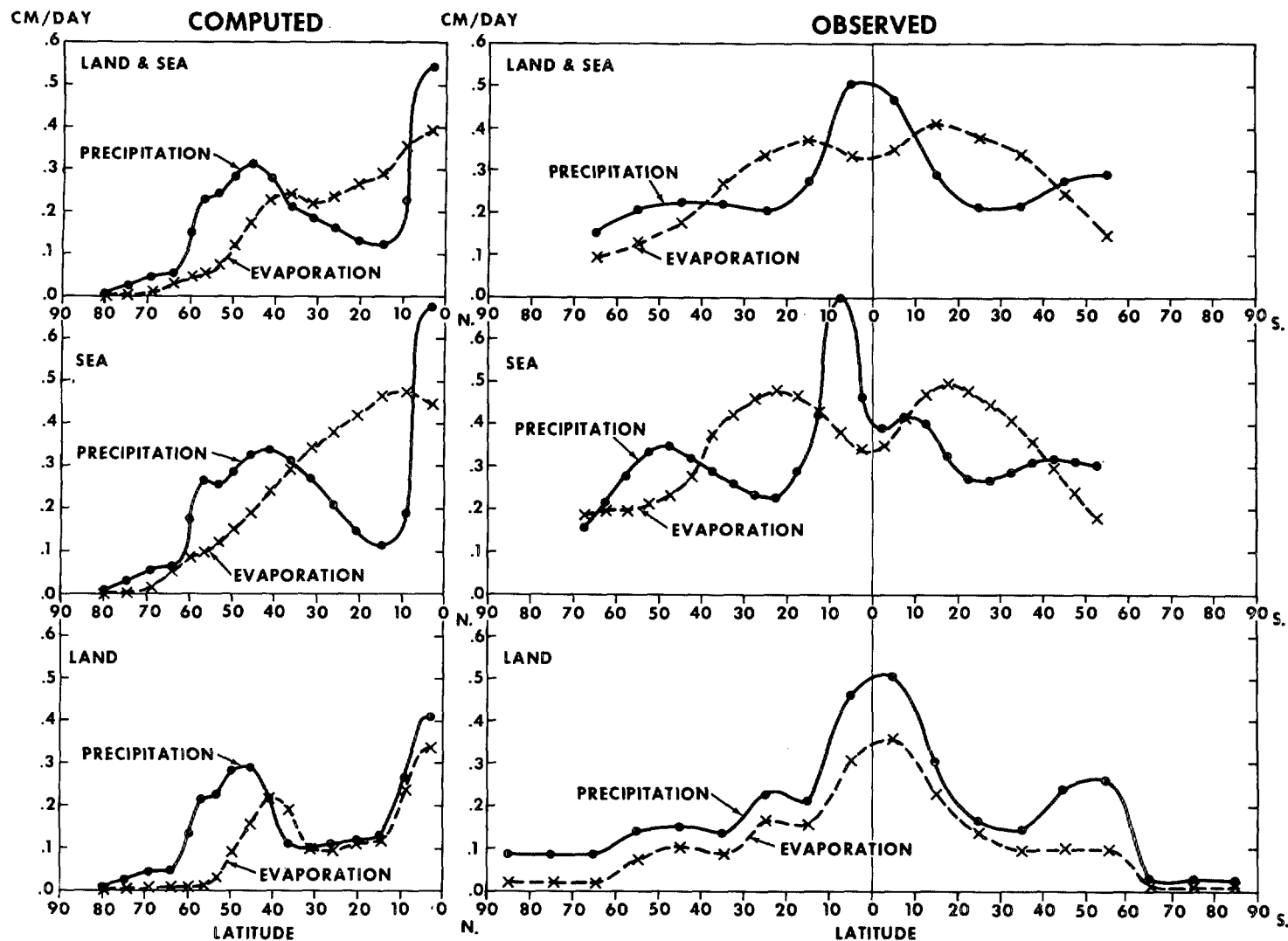


FIGURE 23.—Latitudinal distributions (computed and observed) of zonal mean precipitation and evaporation; the distribution of the model (computed) is obtained by taking the average of the two hemispheres.

of moisture transport in the model atmosphere and the actual atmosphere are plotted. The major features of the distribution of the integrated moisture transport in the model atmosphere (left diagram) are as follows.

From the source region of the subtropical ocean, moisture moves southwestward and converges into the tropical rain belt on the ocean. Part of this moisture moves westward and supplies moisture for the tropical rain belt on the continent. Another part moves along the periphery of the oceanic anticyclone, described in subsection 4B, and brings moist air to the east coast of the continent from the Tropics. Thus, it supplies the moisture for the rainy region along the east coast of the continent in the subtropics described earlier.

In the latitude belt ranging from 30° to 50° , the relative magnitude of the westward component of the moisture transport vector is very large. From 45° latitude, the vectors tend to point poleward, and their length decreases rapidly with increasing latitude. The convergence of moisture that results from this distribution accounts for the moisture needed for maintaining the rain belt in middle latitudes.

These features are in excellent qualitative agreement with the moisture transport in the actual atmosphere shown in figure 30B. (It should also be pointed out that the distribution of moisture transport vectors corresponds very closely to the distribution of the wind vectors near the earth's surface, fig. 12.) There are, however, significant quantitative differences. For example, the length of the moisture transport vector of the polar region is much smaller in the model atmosphere than in the actual atmosphere. This is probably because the temperature of the polar region of the model atmosphere is significantly lower than that of the actual atmosphere, as shown in subsection 3A.

F. GENERAL CIRCULATION AND SURFACE HYDROLOGY

The general circulation of the atmosphere controls the hydrology of the earth's surface. In return, the surface hydrology affects the general circulation. We shall discuss a few examples of the interactions of this sort.

Desert-forming mechanism.—It is interesting that in the subtropics the area with small amounts of rainfall has a wider latitudinal spread on the continent than over the

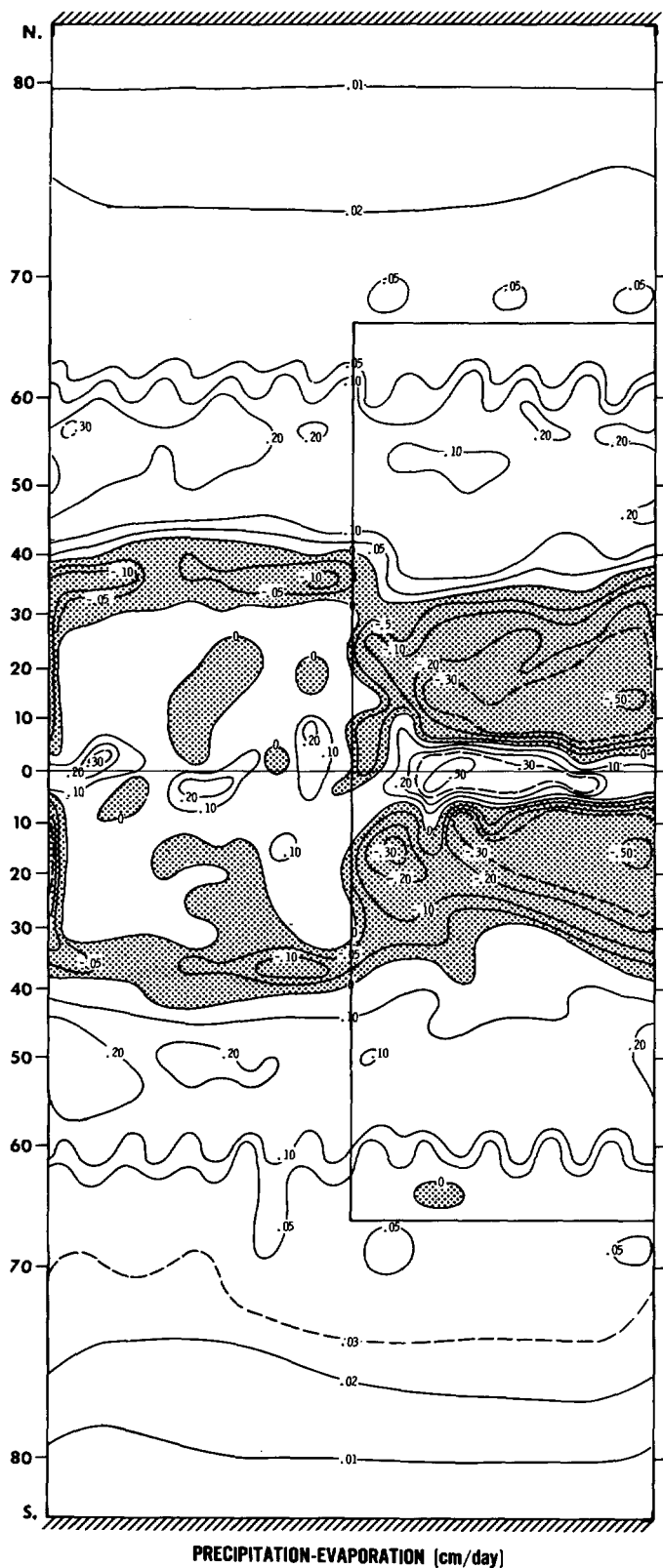


FIGURE 24.—Horizontal distribution of the difference ($P - E$) between precipitation and evaporation of the model.

ocean. This is a result of the self-amplification mechanism, which plays an important role in desert formation. In general, the rainfall is meager in the subtropics because the downward branch of the direct cell of meridional circulation prevails there. When the rate of rainfall is

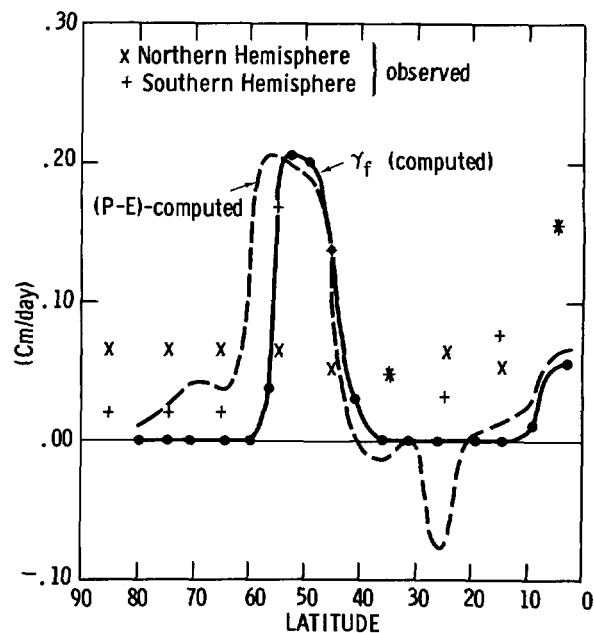


FIGURE 25.—Latitudinal distributions of $(P - E)$ and runoff (γ_f) of the model, obtained by taking the average of the two hemispheric distributions. Values of runoff obtained by Lvovitch and Ovtchinnikov (1964) are also plotted.

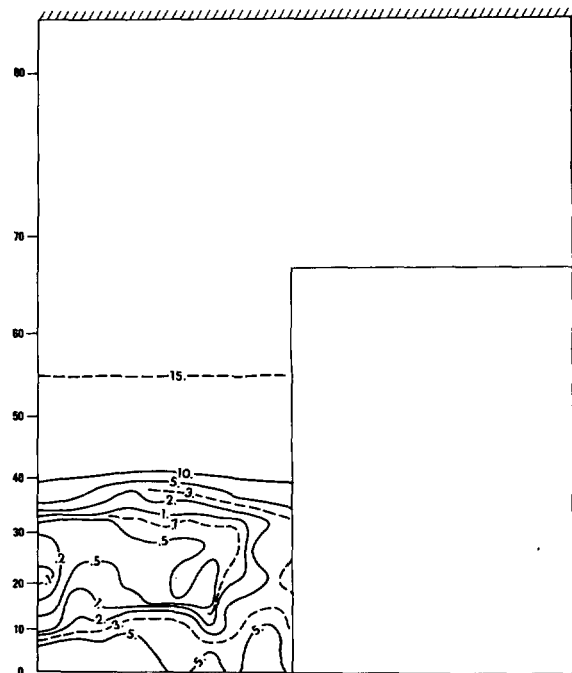


FIGURE 26.—Horizontal distribution of soil moisture (centimeters) of the model. The values of the two hemispheres are averaged.

smaller on the land surface, then the soil moisture is less and accordingly the rate of evaporation is less. In turn, this small evaporation rate is responsible for the decrease in relative humidity in the lower troposphere and then for the further decrease in rainfall and soil moisture. On the other hand, moisture is always abundant in the ocean area. This kind of self-amplification mechanism does not exist over the subtropical ocean; therefore, the belt of

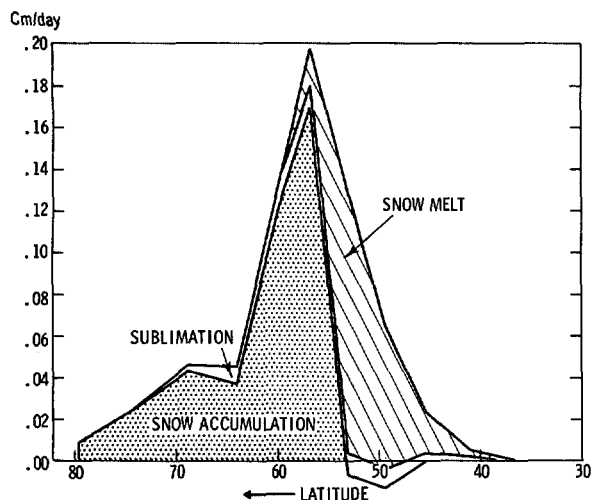


FIGURE 27.—Latitudinal distribution of the zonal mean snow budget on the continent of the model. The values of the two hemispheres are averaged. The negative rate of accumulation around latitude 50° indicates the decrease of snow depth during the period of time averaging.

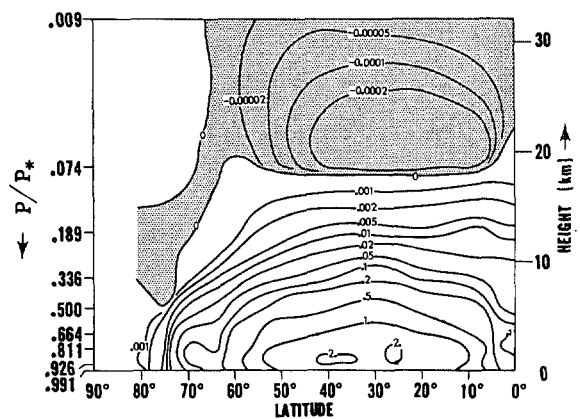


FIGURE 29.—Latitude-height distribution of poleward transport of water vapor by transient eddies in the model atmosphere (units, $10^{14} \text{ gm mb}^{-1} \text{ day}^{-1}$). The distributions of the two hemispheres are averaged.

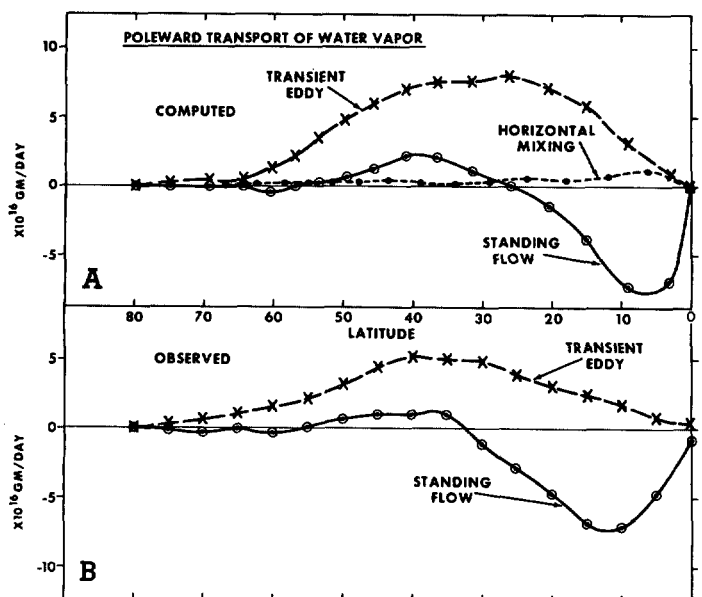


FIGURE 28.—Latitudinal distributions of poleward transport of water vapor due to various processes; (A) the distributions in the model atmosphere (average of the two hemispheres) and (B) the distributions of the actual atmosphere (Northern Hemisphere).

meager rainfall is naturally narrower over the ocean than over the continent in the subtropics.

East coast rainfall in the subtropics—As we have already described, the belt of meager rainfall in the subtropics is interrupted by an area of relatively abundant precipitation along the east coast of the continent. We shall discuss the mechanism maintaining a distribution of this sort.

In the subtropical desert, the rate of evaporation is very small. Instead, the turbulent transport of sensible heat prevails to compensate for the gain of energy due to incoming solar radiation. Accordingly, the temperature

of the desert area is very high. Figure 7 shows the temperature distribution of the ninth model level (about 70 m). The high desert temperature in turn develops the area of low surface pressure because of the relatively low air density near the earth's surface. On the other hand, the surface temperature of the subtropical region of the ocean is relatively low because of the rapid evaporation from the oceanic surface. Thus, an area of relatively high surface pressure develops in the oceanic region of the subtropics (fig. 9A). This oceanic anticyclone causes the tropical air to move poleward along the east coast of the continent in the subtropics. The distribution of the vertical integral of the moisture transport vector (fig. 30) clearly indicates such a poleward transport. Therefore, a moist tongue of tropical air covers the east coast region of the subtropics. The cross section of humidity distribution along 20.5° N . latitude in figure 31 clearly indicates this moist tongue. The distribution of the vertical integral of vertical motion (fig. 32) also favors the maintenance of this moist air mass in the lower half of the troposphere. Despite the general predominance of downward motion in the subtropics, weak upward motion appears along the east coast and tends to increase the relative humidity there. This moist tongue constitutes a favorable environment for cyclogenesis and, consequently, abundant precipitation along the east coast of the continent in the subtropics. (See section 8 for further discussion on the mechanism of cyclogenesis.)

Time mean vertical motion—The influence of surface hydrology upon the atmospheric circulation, which we have discussed so far, is evident in the distribution of the time mean vertical motion.

Figure 33 shows the zonal mean motion (time mean) on both land and sea. On the subtropical ocean, the downward branch of the direct cell extends uniformly throughout the troposphere; whereas on the subtropical continent, a region of upward motion appears near the earth's surface at 10° to 20° latitude (fig. 32). This local upward motion probably resulted from the intense heating by sensible

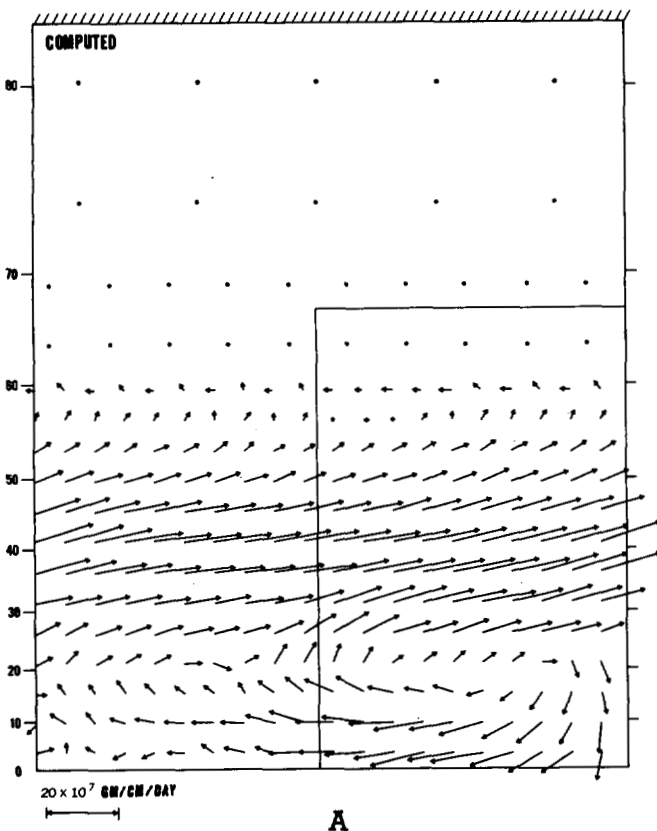
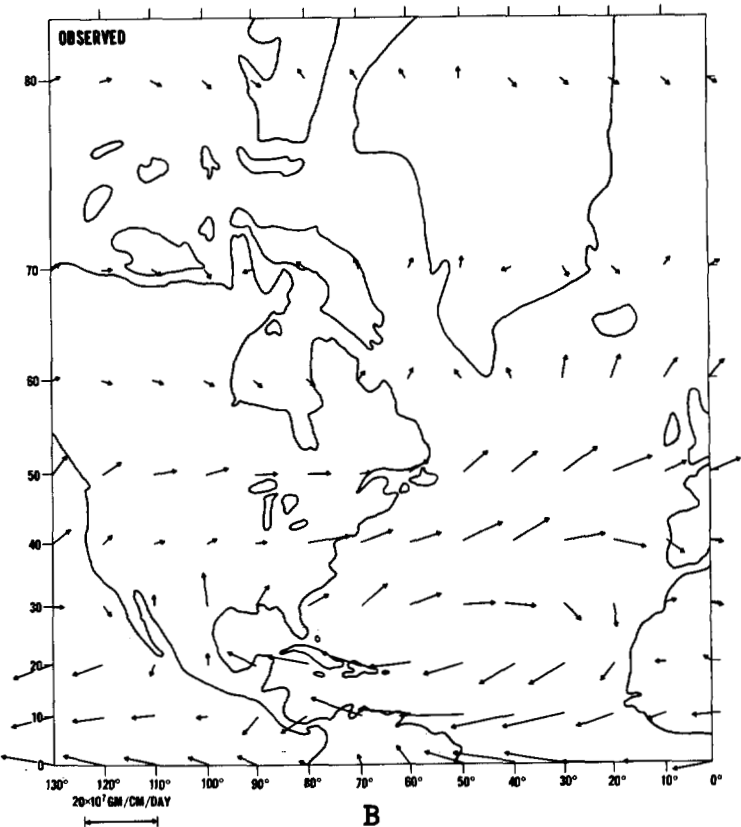
**A****B**

FIGURE 30.—Vertical integral (pressure-weighted) of the moisture transport vector; (A) the distribution in the model atmosphere (average of the two hemispheres) and (B) the distribution in the actual atmosphere (Northern Hemisphere) obtained by Peixoto and Crisi (1965).

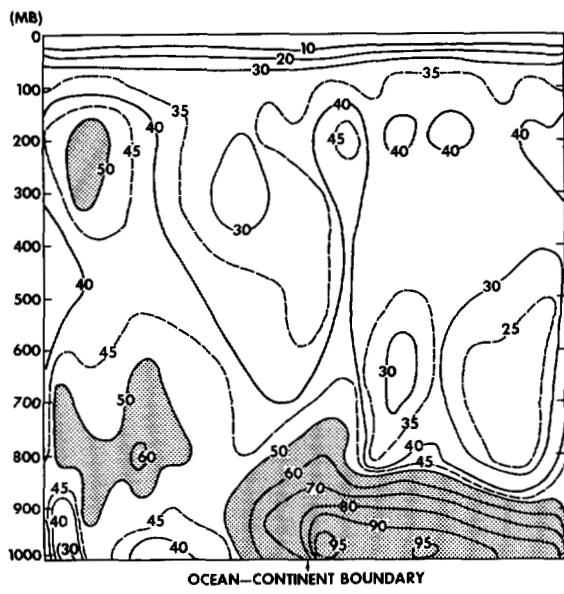


FIGURE 31.—Zonal cross-section of relative humidity in percent along the 20.5° latitude circle.

heat from the hot desert surface. As we demonstrate in part II, the temperature of the earth's surface seems to have a very important effect upon the time mean vertical motion.

Another feature of interest is the comparison of the relative intensity of the Hadley circulation on the continent and on the ocean. The upward branch of the tropical

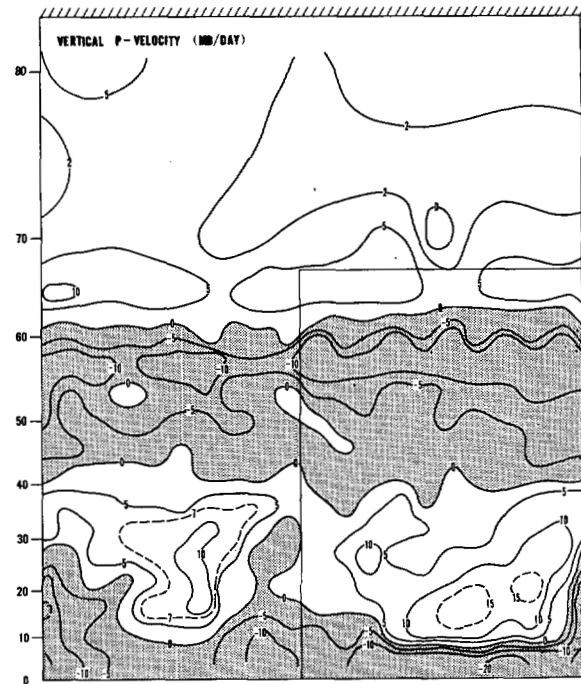


FIGURE 32.—Horizontal distribution of vertically integrated (pressure-weighted) vertical P -velocity of the model. The distributions of the two hemispheres are averaged.

meridional circulation cell is weaker on the continent than on the ocean. As pointed out in study M, water vapor plays an important role in accelerating this direct cell.

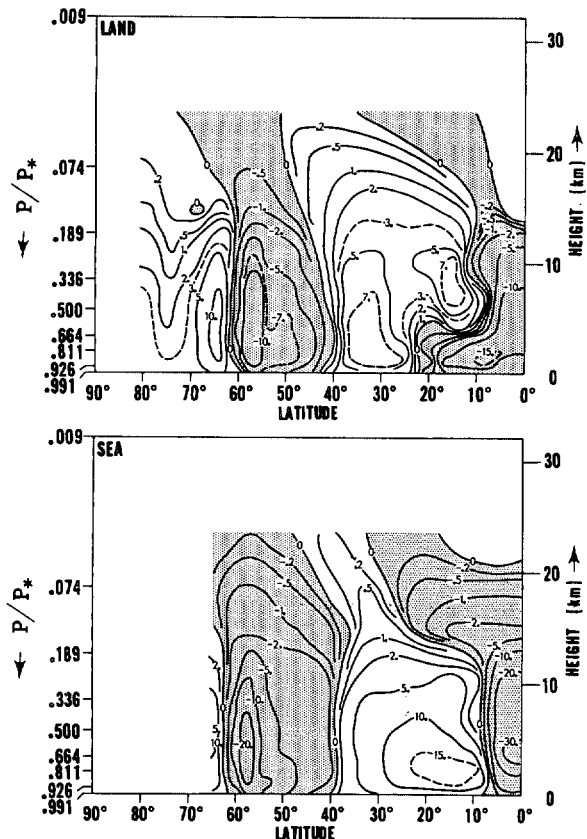


FIGURE 33.—Latitude-height distributions of zonal mean vertical P -velocity (mb day^{-1}) over the continent and ocean of the model. The distributions of the two hemispheres are averaged.

An insufficient supply of moisture from the continental surface may be responsible for the weak Hadley cell over the continent. This relative intensity is altered significantly when the effect of the ocean circulation is taken into consideration. We shall discuss this subject in part II.

G. WATER BALANCE OF THE EARTH'S SURFACE

The diagram of the water balance is shown in figure 34, thus concluding this section. Despite the idealization of the land-sea configuration in the model, the agreement between the magnitudes of most of the water balance components of the model and those estimated by Budyko (1963) from actual data is generally good. The intensity of the hydrologic cycle, however, is slightly stronger in the actual atmosphere than in the model atmosphere.

7. HEAT BALANCE

A. RADIATION BALANCE OF THE EARTH-ATMOSPHERE SYSTEM

The areal distribution of net radiative fluxes at the top of the atmosphere is given in figure 35. In this figure, the net solar radiation is generally smaller over the continent than over the ocean due to the difference in surface albedo. Particularly, the sudden increase of net solar radiation from the continent to the ocean around 60° latitude is caused by the large albedo of snow cover on the continent.

The net upward long-wave radiation is a maximum in the subtropical region of the continent where the tempera-

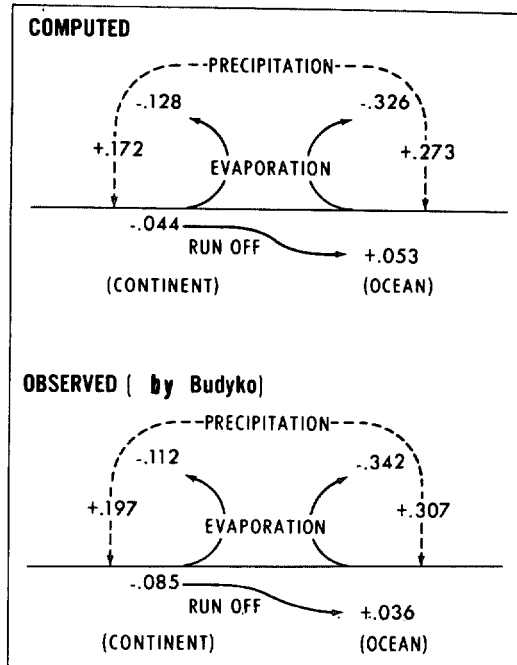


FIGURE 34.—Computed and observed water balance of the earth's surface (units, cm day^{-1}).

ture of the soil surface is high. Around 60° latitude, the surface temperature of the oceanic area is much higher than the surface temperature of the continental area due to the differences in surface albedo. This relatively warm temperature of the ocean surface is mainly responsible for the marked increase of long-wave radiation from the continent to the ocean in this latitude.

The distribution of radiation imbalance of the earth-atmosphere system is computed as the difference between net downward solar radiation and net upward long-wave radiation at the top of the atmosphere (fig. 36). Also shown, for comparison, is the corresponding distribution for the actual atmosphere obtained by Budyko (1963). In figure 36, the positive radiation imbalance of the model subtropics is less in the land area than in the sea area. As we have pointed out, this longitudinal gradient of imbalance is caused by the relatively large emission of long-wave radiation from the hot desert surface and by the relatively large reflection of solar radiation from the continental surface whose albedo is higher than the albedo of the ocean. Although this feature is in qualitative agreement with Budyko, it is somewhat exaggerated due partly to the lack of longitudinal variation of cloudiness in the model. In higher latitudes (60°), a sharp land-sea contrast in the value of radiation imbalance exists due to the large albedo of snow, which covers the land area. Such a sharp contrast does not exist in the observed distribution, because the latitude of the actual snow line is much higher than the one in the model, except during winter.

Figure 37 depicts the latitudinal distributions of the zonal mean values of net solar and long-wave radiation at the top of the model atmosphere. The distributions for the actual atmosphere obtained by London (1957) are shown for comparison. This figure clearly shows that, in high latitudes, both net solar radiation and net long-wave

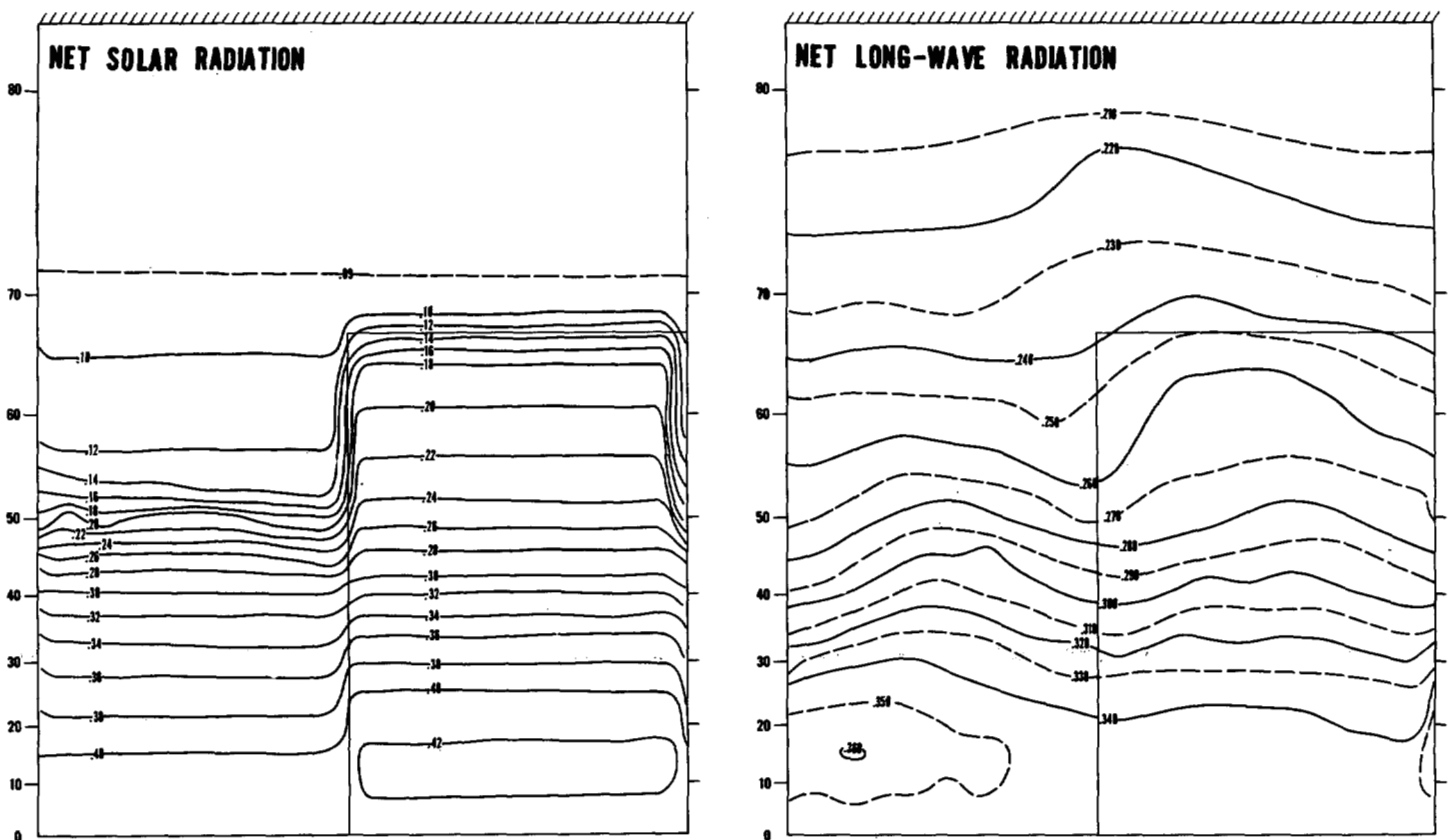


FIGURE 35.—Horizontal distributions of net downward solar radiation and net upward long-wave radiation at the top of the model atmosphere (units, ly min⁻¹). The distributions of the two hemispheres are averaged.

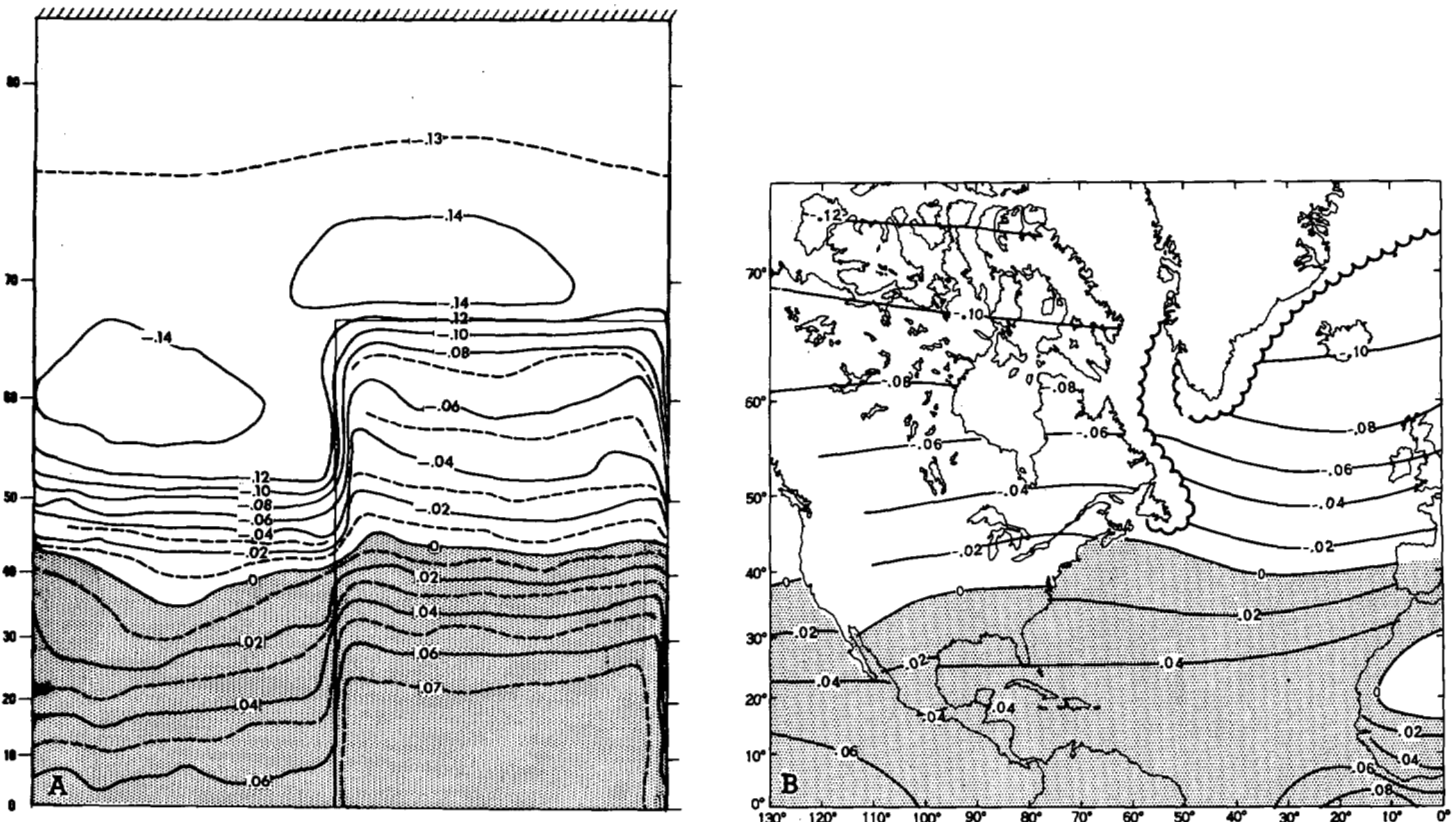


FIGURE 36.—Horizontal distribution of net downward radiation at the top of the atmosphere (radiation imbalance of the earth-atmosphere system); (A) distribution for the model (average distribution for the two hemispheres) and (B) distribution for the actual atmosphere, estimated by Budyko (1963); units, ly min⁻¹.

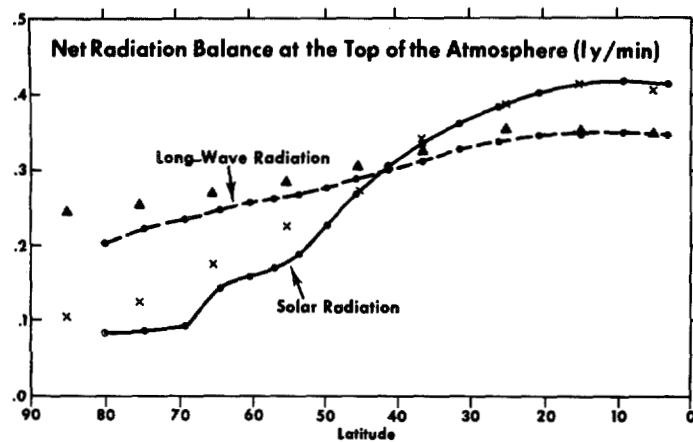


FIGURE 37.—Zonal means of the net downward solar radiation at the top of the model atmosphere and of the actual atmosphere are indicated by a solid line and x's, respectively. Zonal means of the net upward long-wave radiation at the top of the model atmosphere and the actual atmosphere are indicated by a dashed line and solid triangles, respectively. The values of the two hemispheres of the model are averaged. The estimates of the actual radiative fluxes in the Northern Hemisphere were obtained from London (1957).

radiation are too small at the top of the model atmosphere, though the difference between the two is quite realistic. As discussed, these small radiative fluxes are caused by the extensive snow cover of the model. In other words, we effectively have the climate of an ice age.

B. POLEWARD TRANSPORT OF ENERGY

The radiative imbalance of energy requires the poleward transport of energy. In the actual system, this is accomplished by the following three processes:

- 1) atmospheric transport of heat energy ($c_p T + \phi + K$),
- 2) atmospheric transport of latent energy ($L \cdot r$), and
- 3) oceanic transport of heat.

Since the effect of heat transport by ocean currents is not incorporated in the present model, the total heat transport can only be accomplished by the first two mechanisms. Figure 38A shows how the poleward transport of energy required from radiative imbalance is partitioned between these two means of transporting energy. For comparison, the poleward transport of energy by the actual earth atmospheric system is shown in figure 39. It is interesting that the magnitude of poleward transport of energy required from radiative imbalance in the model atmosphere is very close to that in the actual atmosphere despite the very low temperatures of the polar region. As figure 37 shows, snow cover in high latitudes has the effect of decreasing both net downward solar radiation and net upward radiation simultaneously. Therefore, the net radiative imbalance is affected very little. The magnitude of poleward transport of heat energy ($c_p T + \phi + K$) agrees reasonably well with the estimate for the actual atmosphere. The poleward transport of latent energy, however, is somewhat larger than the estimates obtained by Peixoto (1958).

Figures 38B, C show a further breakdown of these transports. Both the transport of heat energy and the

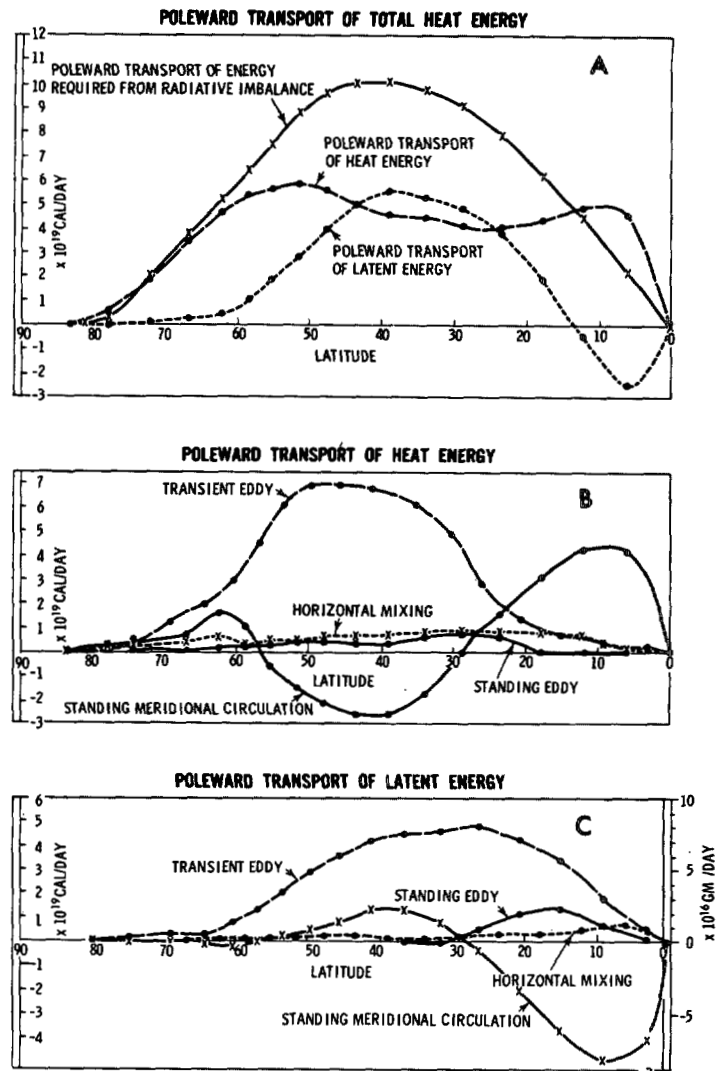


FIGURE 38.—(A) latitudinal distribution of the net poleward transport of energy required from radiative imbalance, and the poleward transport of heat energy and latent energy; (B) the latitudinal distribution of the poleward transport of heat energy; and (C) the latent energy due to various processes such as transient eddies, standing eddies, standing meridional circulations, and subgrid scale mixing.

transport of latent energy are subdivided into four processes, that is, the transport by transient eddies, standing eddies, the standing meridional circulation cell, and subgrid scale mixing.

In figure 38, the direct cell of the meridional circulation in low latitudes brings latent energy into the Tropics and exports large amounts of heat energy from the Tropics. In this way it plays a major role in maintaining the tropical rain belt. The tropical maximum of poleward transport of heat energy evident in figure 38A is caused by this direct cell.

In the middle latitudes, transient eddies play a major role in transporting both heat energy and latent energy poleward. The eddy transport of latent energy is a maximum around 30° latitude; whereas the eddy transport of heat energy is a maximum around 45° and is responsible for the high-latitude maximum of total poleward transport

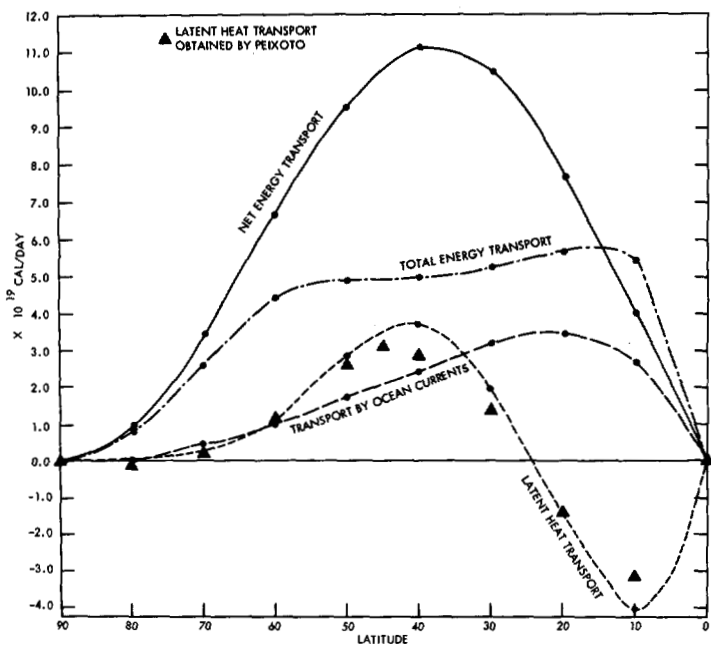


FIGURE 39.—Latitudinal distribution of the net poleward transport of energy by the joint ocean-atmosphere system, expected from radiative imbalance, is indicated by a solid line. The transport of total energy ($c_p T + \phi + K$) and that of latent energy in the atmosphere are shown by a dash-dot line and a dashed line, respectively. The energy transport by ocean currents is also included. The estimate of these transports was made using the data obtained by Budyko (1956, 1963) and Houghton (1954). Budyko's data for the two hemispheres are averaged. The meridional transport of latent energy obtained by Peixoto (1958) is plotted for comparison.

of heat energy shown in the upper part of figure 39. The indirect cell of the meridional circulation plays a minor role in middle latitudes. It transports heat energy equatorward and latent energy poleward.

In general, the contribution of standing eddies is small in the model atmosphere. Since mountains excite standing eddies, this may not be the case in the actual atmosphere.

The latitude-height distributions of the poleward transport of heat ($c_p T$) and of heat energy ($c_p T + \phi + K$) by transient eddies are shown in figures 40A, B, respectively; they have double maxima in middle latitudes, one near the 900-mb level and another near the 200-mb level. Similar double maxima are evident in figure 41, which shows the observed distribution of poleward transport of heat by the transient eddies. The latitude-height distribution of transport of heat energy in the actual atmosphere is not available. In view of the significant difference between the transport of heat energy and the transport of heat, it would be very valuable to obtain an estimate of the poleward transport of geopotential height ϕ for the actual atmosphere.

For the latitude-height distribution of latent energy transport, refer to figure 29.

C. RADIATION BALANCE OF THE EARTH'S SURFACE

The horizontal distribution of net downward solar radiation at the earth's surface is shown in the left diagram

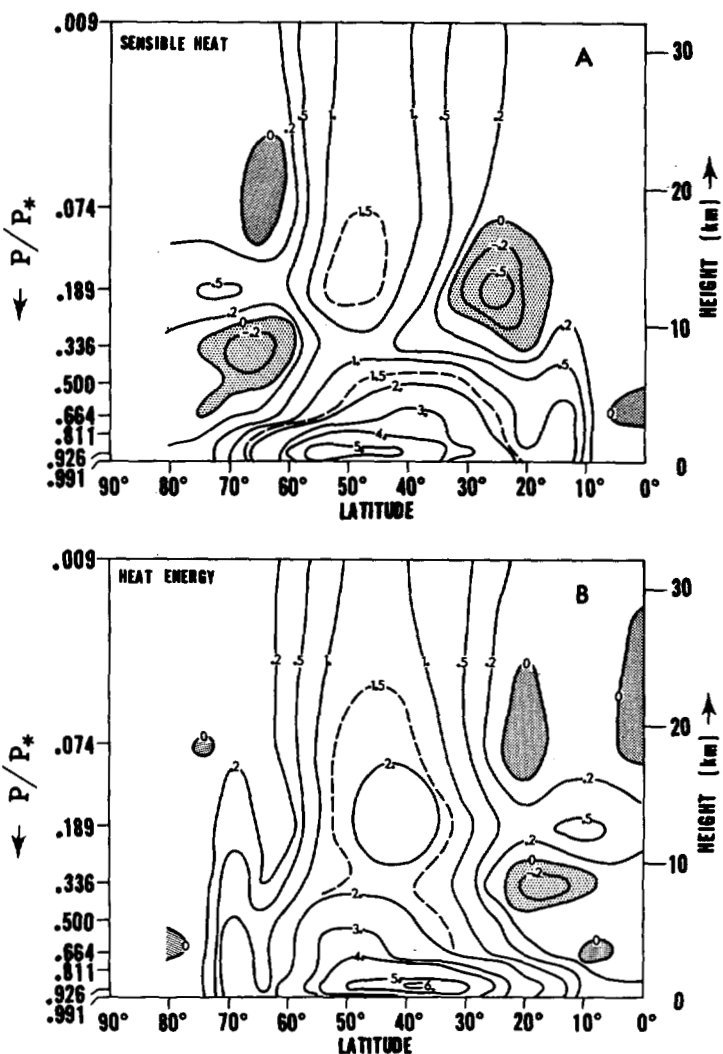


FIGURE 40.—Latitude-height distribution of (A) the poleward transport of heat ($c_p T$) and (B) the poleward transport of heat energy ($c_p T + \phi$) (the transport of kinetic energy is neglected). The values of the two hemispheres are averaged (units, 10^{17} joules $\text{mb}^{-1} \text{day}^{-1}$).

of figure 42. In this figure, the net solar radiation is generally larger over the ocean than over the continent, due to the difference in the surface albedo. Near 60° latitude, the contrast in net radiation is particularly distinct because of the large albedo of snow cover on the continent.

The horizontal distribution of net upward long-wave radiation at the earth's surface is shown in the right diagram of figure 42. In the subtropical desert region of the model, the net upward long-wave radiation is significantly larger than the surrounding region due to the high temperature of the soil surface. Near 60° latitude, a significant difference in flux between ocean and continent exists due to the difference in surface temperature and in vertical temperature gradient near the earth's surface.

The latitudinal distribution of the zonal mean value of radiative fluxes at the earth's surface is shown in figure 43. For comparison, the annual mean fluxes estimated by London (1957) for the actual atmosphere are also shown. In lower latitudes, both net solar and net long-wave

radiation agree very well with London's estimate for the actual atmosphere; in higher latitudes, however, the radiative fluxes of the model are significantly less than those of the actual atmosphere. This is due to the effect of excessive snow cover.

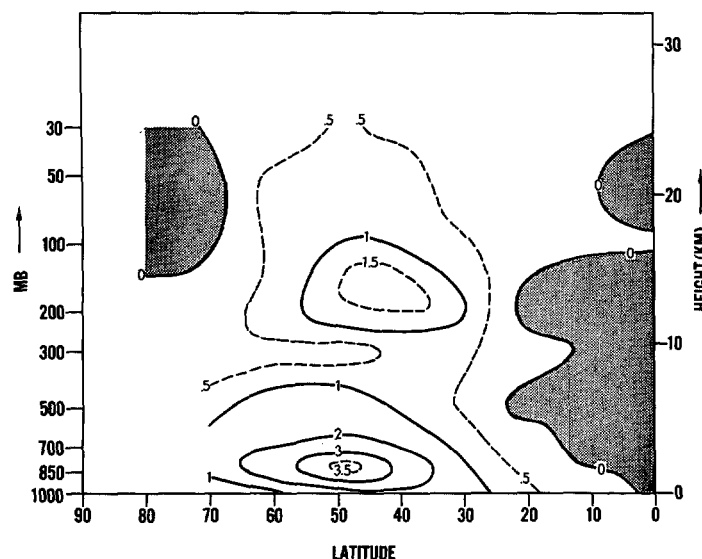


FIGURE 41.—Latitude-height distribution of poleward transport of heat in the actual atmosphere (Peixoto, 1958); units, 10^{17} joules $\text{mb}^{-1} \text{day}^{-1}$.

The distribution of radiation imbalance (net downward radiation) at the earth's surface is computed as the difference between net downward solar radiation and net upward long-wave radiation and is compared with Budyko's estimated distribution in figure 44. In general, the radiation imbalance is positive except for very high latitudes. Due to high surface temperature and associated large upward long-wave radiation, the positive imbalance in the subtropics is significantly smaller over land than over the sea, in agreement with the observed features. In higher latitudes, the magnitude of imbalance on the continent is much smaller than on the ocean because of the large reflectivity of snow cover for solar radiation. Although this feature is in qualitative agreement with observation, the contrast between land and sea is too exaggerated in the model. Actual snow cover extends widely only during winter; whereas, it extends as far south as 53° latitude in the model atmosphere.

In figure 45, the latitudinal distributions of zonal mean radiative imbalance for both the continent and ocean (model) are contrasted with those estimated by Budyko (1963). In low latitudes the agreement with Budyko's result is reasonably good; whereas in high latitudes there are some systematic differences, probably due to the effect of excessive snow cover. Nevertheless, the difference between the imbalance for the model and for the actual atmosphere is small if one takes the average for both land and sea.

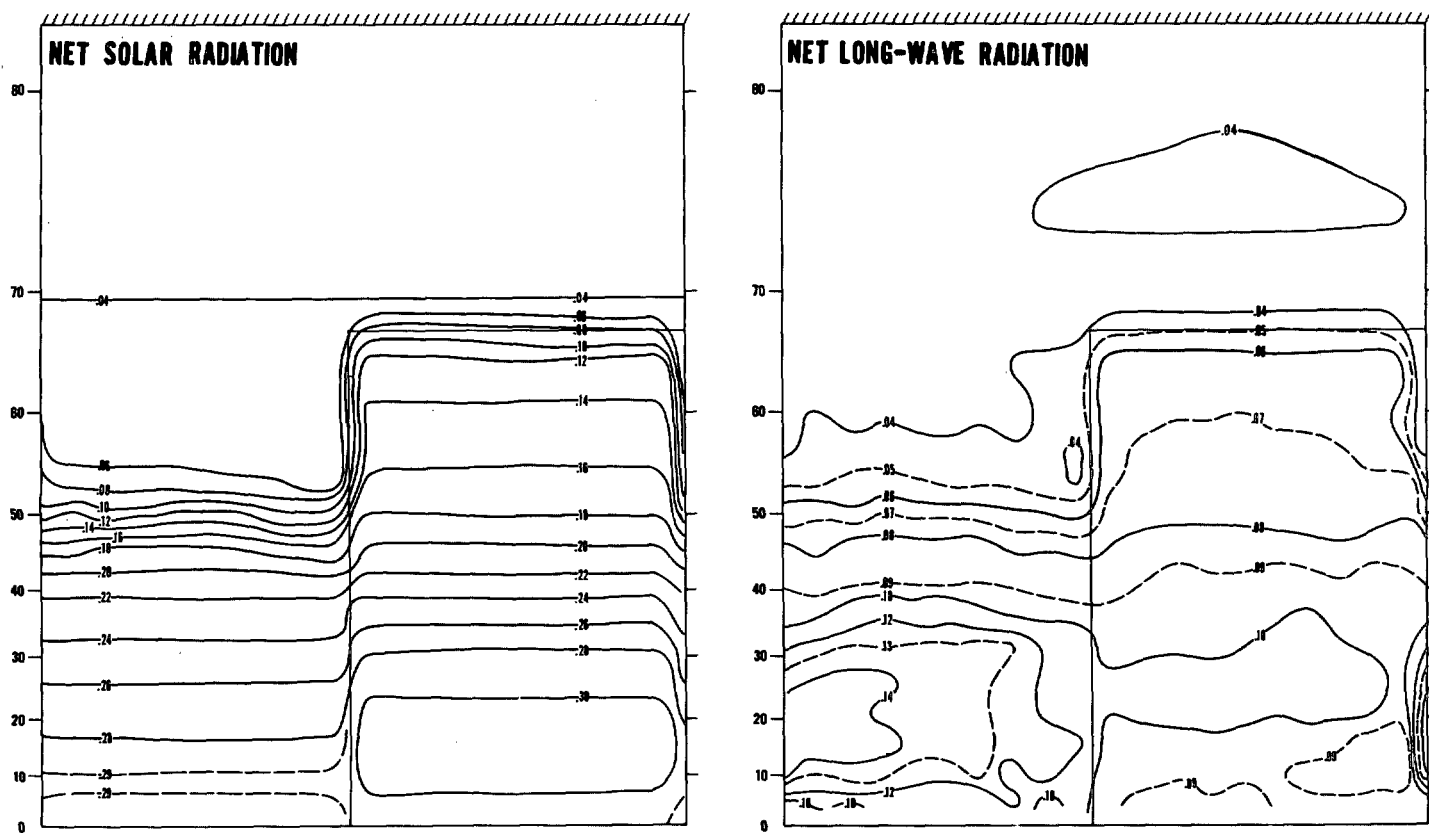


FIGURE 42.—Horizontal distributions of net downward solar radiation and of net upward long-wave radiation at the earth's surface of the model (average of two hemispheric values). Units, ly min^{-1} .

D. TURBULENT FLUX OF SENSIBLE AND LATENT HEAT

In the left parts of figure 46, the model distributions of the zonal mean values of both sensible and latent heat flux at the earth's surface are shown for both the continent and the ocean. In the right parts of the same figure, the corresponding quantities as estimated by Budyko (1963) are shown for comparison.

On the ocean surface of the model, the magnitude of the flux of latent heat decreases with increasing latitude,

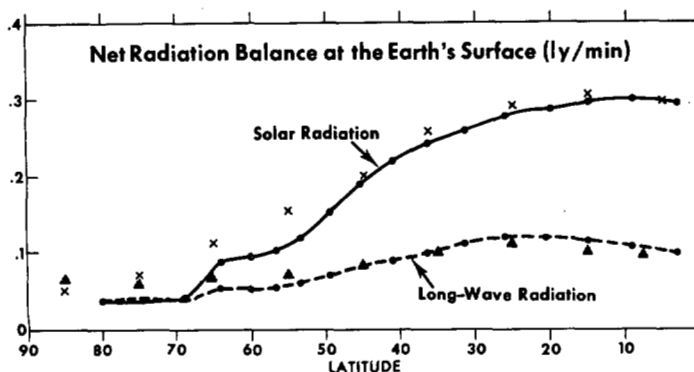


FIGURE 43.—Zonal means of the net downward solar radiation at the surface of the model earth and of the actual earth are indicated by a solid line and x's, respectively. Zonal means of the net upward long-wave radiation at the surface of the model earth and of the actual earth are indicated by a dashed line and solid triangles, respectively. The values of the two hemispheres of the model are averaged. The estimates of actual radiative fluxes in the Northern Hemisphere were obtained from London (1957).

except in the Tropics, whereas the magnitude of sensible heat flux increases with increasing latitude. As pointed out in study M, this results in an increase in Bowen ratio with increasing latitude in qualitative agreement with the actual distribution estimated by Jacobs (1951). It is reasonable that, in high latitudes, latent heat flux should play a minor role in removing the heat from the ocean surface because the vertical gradient of vapor pressure is generally small due to the low temperature. The distributions of sensible and latent heat flux over the ocean are very similar to those obtained in study M in which the earth's surface was assumed to be completely wet.

On the surface of the continent, the rate of evaporation decreases sharply from the Tropics to the subtropics due to the decrease of soil moisture. This decrease is compensated by the latitudinal increase of the sensible heat flux. Despite the drastic idealization of land-sea configuration adopted for this study, these features of flux distribution of the model are in excellent agreement with those obtained by Budyko (1963).

In figure 47, the horizontal distributions of both sensible and latent heat flux are shown. This figure clearly shows how these two fluxes tend to supplement each other. For example, the magnitude of latent heat flux is very small in the subtropical desert; whereas the magnitude of sensible heat is very large. The sum of these two quantities in the desert, however, is somewhat smaller than the corresponding sum in the oceanic region of the subtropics and is consistent with the horizontal distribution of radiative imbalance, which has a relatively small value in the desert (fig. 44).

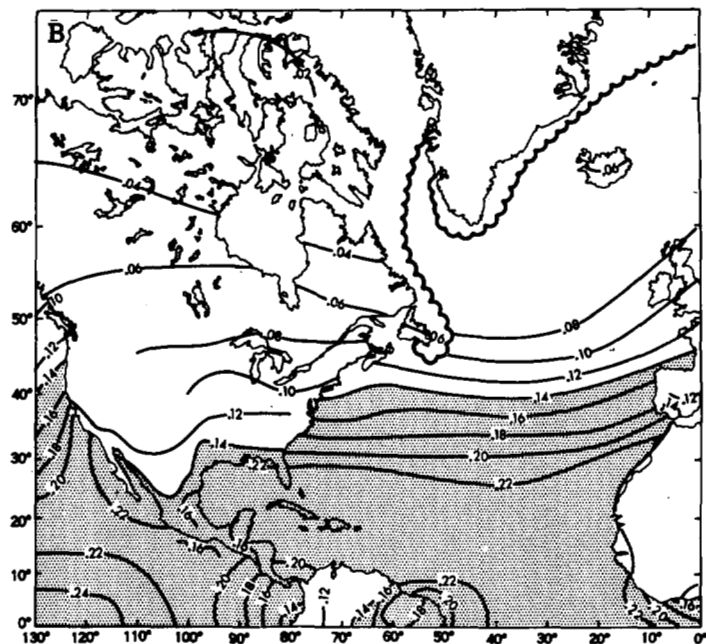
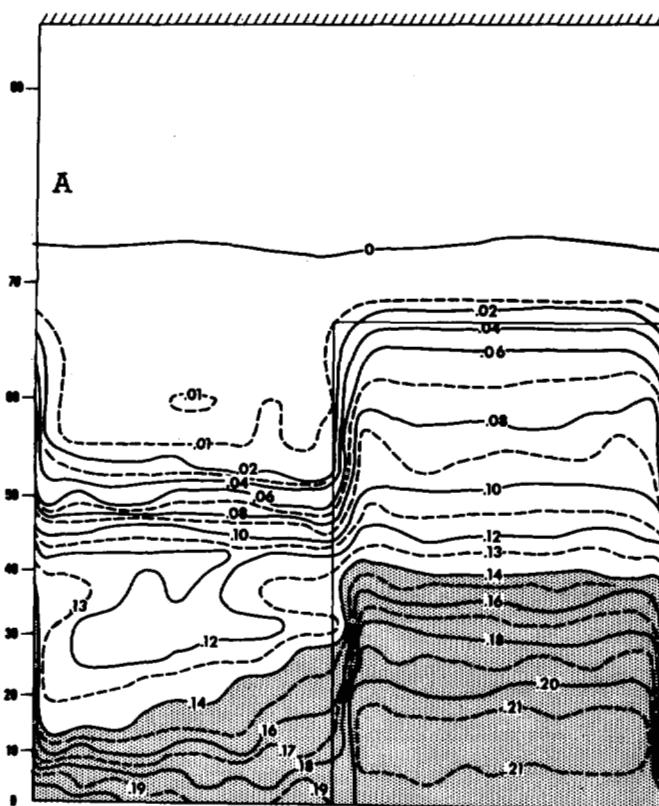


FIGURE 44.—Horizontal distribution of radiation imbalance at the earth's surface; (A) the distribution of the model (average of two hemispheric values) and (B) the distribution of the actual earth's surface, obtained by Budyko (1963); units, ly min^{-1} .

The horizontal distribution of sensible heat flux estimated by Budyko (1963) is shown in figure 48. There are many common features between Budyko's distribution and the distribution of the model—for example: the maximum in the desert, minimum in the tropical ocean, and relatively large flux from the ocean surface in high latitudes. The area of large sensible heat flux off the east coast of the actual continent (around 40° latitude), however, is missing in the model. This is probably due to the lack of advection of warm water by the Gulf Stream. The discussion of the horizontal distribution of latent heat flux, already given in subsection 6A, is not repeated here.

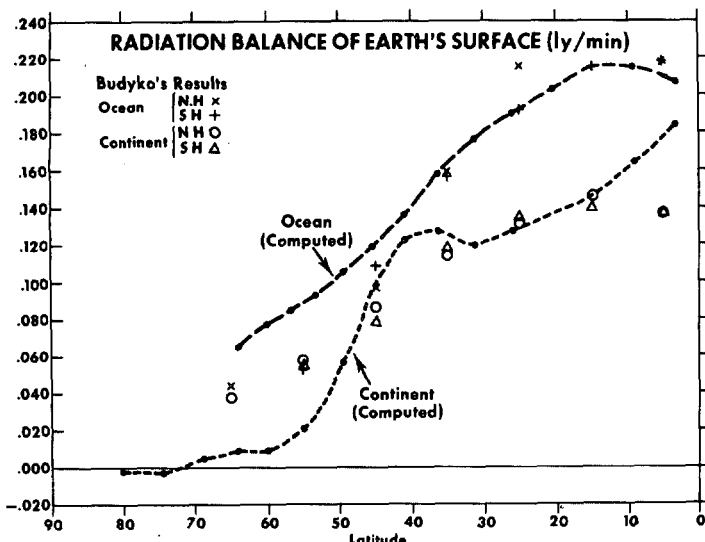


FIGURE 45.—Latitudinal distribution of zonal mean radiation imbalance (average of two hemispheric values) for the continent and ocean separately. The values obtained by Budyko (1963) for the actual earth's surface are plotted for comparison.

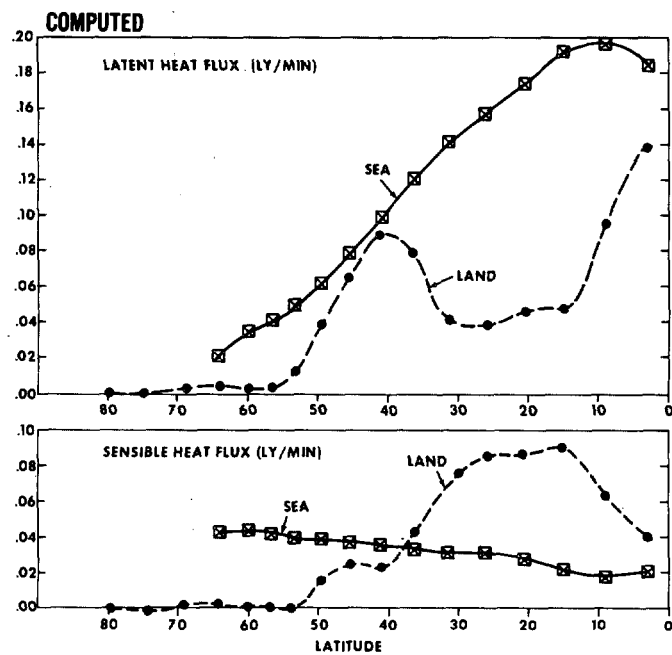


FIGURE 46.—Latitudinal distributions of zonal mean fluxes of sensible and latent heat for the continent and ocean separately. The distributions for the model are shown in the left diagrams (average of two hemispheric values), and the distributions of the actual earth's surface obtained by Budyko (1963) are shown in the right diagrams.

E. HEAT BALANCE DIAGRAM

In concluding this section on the heat balance, diagrams showing the heat balance of the whole earth, the continent, and the ocean are presented in figure 49. According to these diagrams and the water balance diagram of figure 34, both heat energy and latent energy are transported from the ocean to the continent by the atmospheric flow field, probably for two reasons.

1) In general, the albedo of the land surface is larger than the albedo of the ocean. Particularly, snow cover on the continent reflects more solar radiation than the ocean surface.

2) The desert tends to emit relatively large long-wave radiation into space through the window of water vapor absorption bands due to the high temperature there.

In table 2, the heat balance components at the earth's surface of the model are compared with those of the actual atmosphere, estimated by Budyko (1963). Despite the idealized land-sea configuration, the agreement between these two sets of data is surprisingly good.

8. EDDY KINETIC ENERGY

The latitude-height distribution of the zonal mean value of eddy kinetic energy K_E (fig. 50) is defined by

$$K_E = (1/2)[(u - \bar{u}^{\lambda})^2 + (v - \bar{v}^{\lambda})^2].$$

The value of maximum eddy kinetic energy in the middle latitudes is significantly larger than the value as shown in figure 9.2 of study M. This is probably because the meridional temperature gradient is larger in this model than in the previous model because of the extensive development of snow cover in the high latitudes. One of the interesting features of this distribution is the weak maximum of eddy kinetic energy around the Equator.

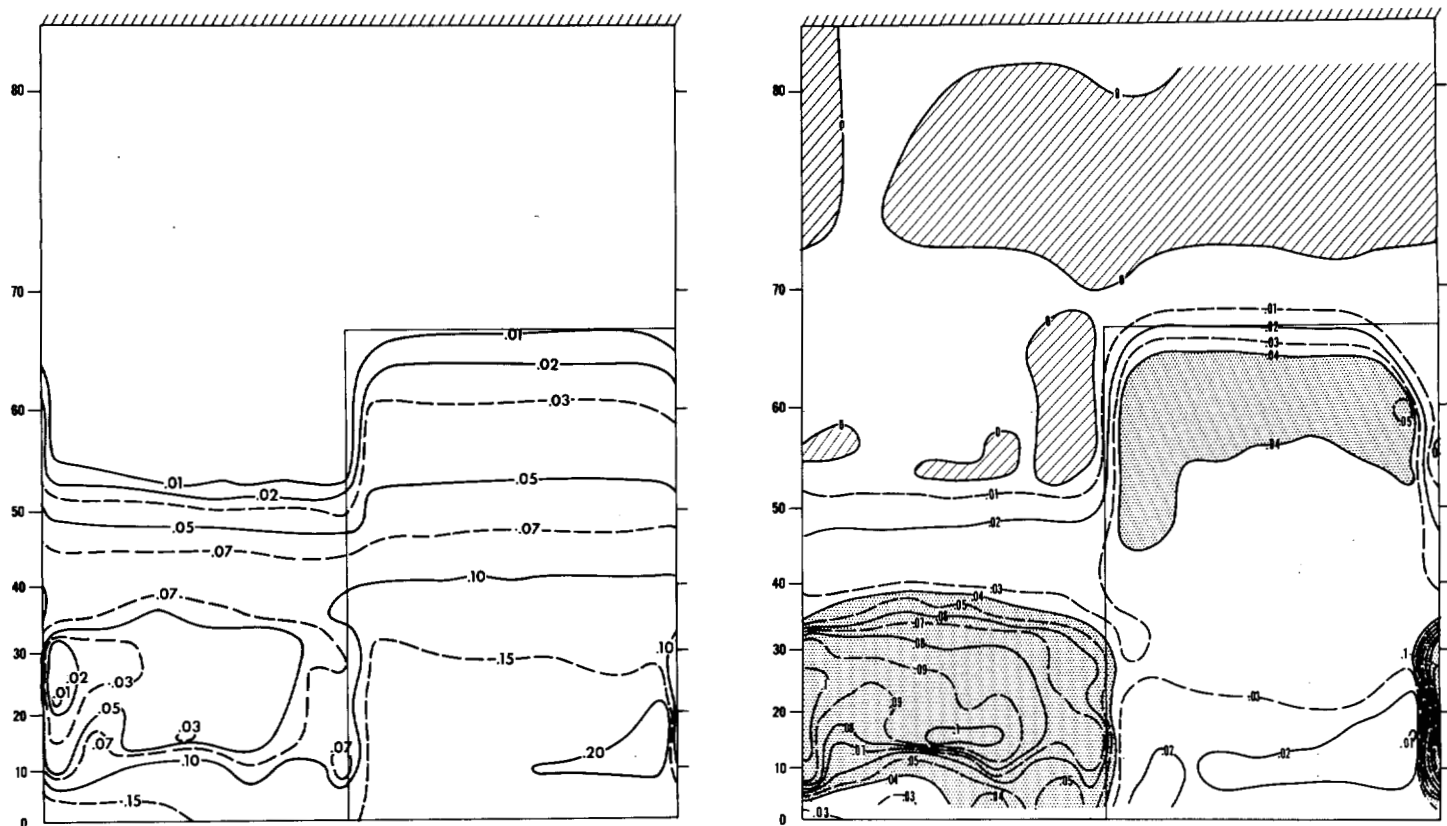


FIGURE 47.—Horizontal distribution of the turbulent flux of latent heat (left diagram) and sensible heat (right diagram), using the average of two hemispheric values; units, ly min^{-1} .

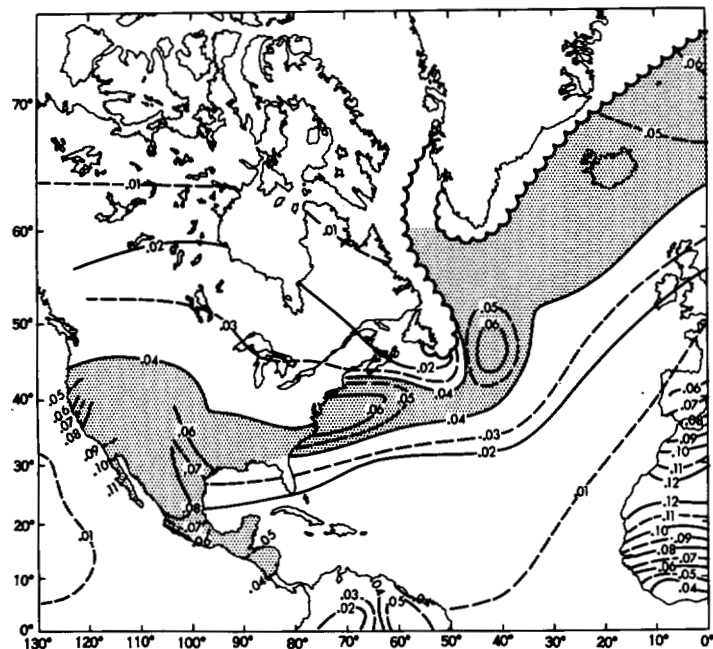


FIGURE 48.—Horizontal distribution of the turbulent flux of sensible heat at the earth's surface, estimated by Budyko (1963); units, ly min^{-1} .

In order to understand this distribution of eddy kinetic energy, the latitude-height distribution of conversion of available potential energy is shown in figure 51. As one would expect, the maximum conversion appears in the middle latitude. Also, a distinct secondary maximum,

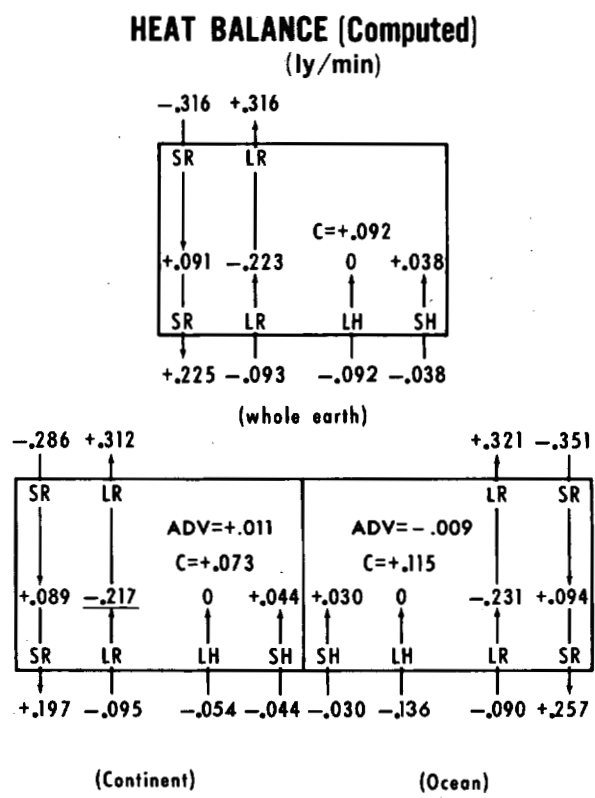


FIGURE 49.—Heat balance diagrams of the model. SR, solar radiation; LR, long-wave radiation; LH, latent heat flux; SH, sensible heat flux; C, heat of condensation; and ADV, advection.

responsible for the tropical maximum of eddy kinetic energy, appears in the upper troposphere of the Tropics.

According to Manabe and Smagorinsky (1967), the conversion of eddy potential energy generated by the heat of condensation is responsible for maintaining the eddy kinetic energy of the model Tropics. Although the resolution of the finite-difference grid in the Tropics is coarser for this study than for study M because of the difference in map projection, the tropical maximum still appeared in this study.

The vertical mean of eddy kinetic energy $\overline{K_E}^P$ is computed by

$$\overline{K_E}^P = \frac{1}{P_*} \int_0^{P_*} K_E dp;$$

its horizontal distribution is shown in figure 52. If one compares figure 52 with the distribution of rainfall in figure 20, he will notice that the area of meager rainfall corresponds to small eddy kinetic energy and the area of

Table 2.—Heat balance of the earth's surface (real earth from Budyko, 1963)

	Whole earth	
	Model earth	Real earth
Radiation balance.....	+ .132	+ .137
Latent heat.....	- .092	- .112
Sensible heat.....	- .038	- .025
Continent		
Radiation balance.....	+ .102	+ .093
Latent heat.....	- .054	- .048
Sensible heat.....	- .044	- .046
Ocean		
Radiation balance.....	+ .167	+ .156
Latent heat.....	- .136	- .141
Sensible heat.....	- .030	- .015

abundant rainfall to large eddy kinetic energy. For example, the eddy kinetic energy is large in the middle latitudes and in the Tropics, where the rate of precipitation is above the average, and small in the subtropics where the rate of rainfall is small. This subtropical belt of minimum eddy kinetic energy is interrupted along the east coast of the continent where the magnitude of eddy kinetic energy and the intensity of rainfall are relatively large.

Similar correspondence between the two quantities holds for time variations as well as for the horizontal distributions. In figure 53, the variation of the latitudinal distribution of vertical and zonal mean eddy kinetic energy with time is contrasted with that of precipitation. Again, the evolution in the distribution of these two quantities correspond very well in the Tropics as well as in the middle latitudes. These results clearly show that rainfall in the model Tropics is mostly accompanied by synoptic scale disturbances, just as in middle latitudes.

The horizontal distribution of the rate of conversion of the eddy available potential energy due to transient eddies is shown in figure 54. Consistent with the zonal mean distribution, areas of large eddy conversion appear in the Tropics and in middle latitudes.

In the subtropics, the conversion of eddy available potential energy due to transient eddies is generally small. In the areas of minimum rainfall, even small negative conversion appears. Along the east coast of the continent, however, the conversion is somewhat larger. It is probable that the moist tongue, occupying this region (fig. 31) and discussed in subsection 6F, constitutes a condition favorable for the generation and development of cyclones. These cyclones, in turn, could be responsible for the ample rainfall in this coastal region. In order to examine this possibility further, figure 55A was constructed. This figure shows the tracks of cyclones generated in the latitude belt ranging from 40° N. to 40° S. during 100

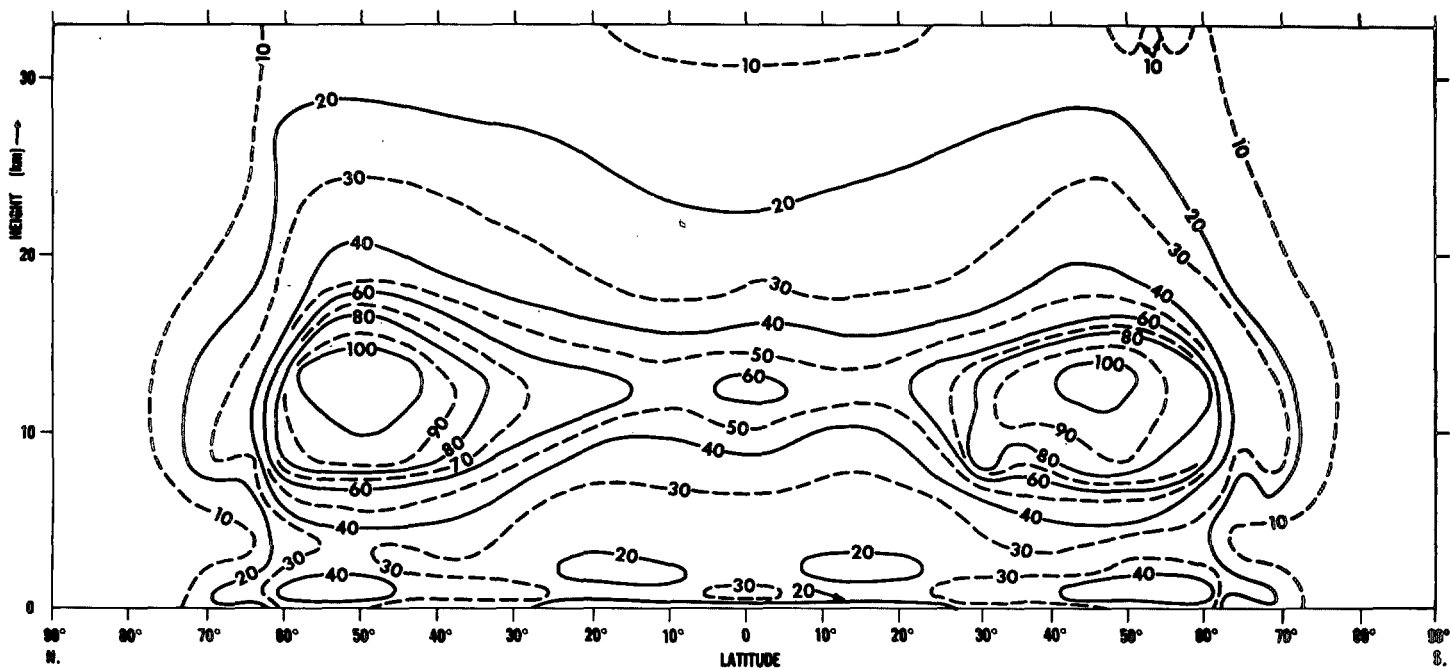


FIGURE 50.—Latitude-height distribution of the zonal mean eddy kinetic energy in the model atmosphere (units, joules $\text{cm}^{-2} \text{mb}^{-1}$).

model days. The figure suggests that the east coast region of the model subtropics is indeed a place favorable for cyclogenesis. The cyclones generated there move poleward and get into the main stream of cyclones in middle latitudes. The poleward movement of the area of maximum rainfall with time, evident in the time isopleths of figure 53, is consistent with this cyclone movement.

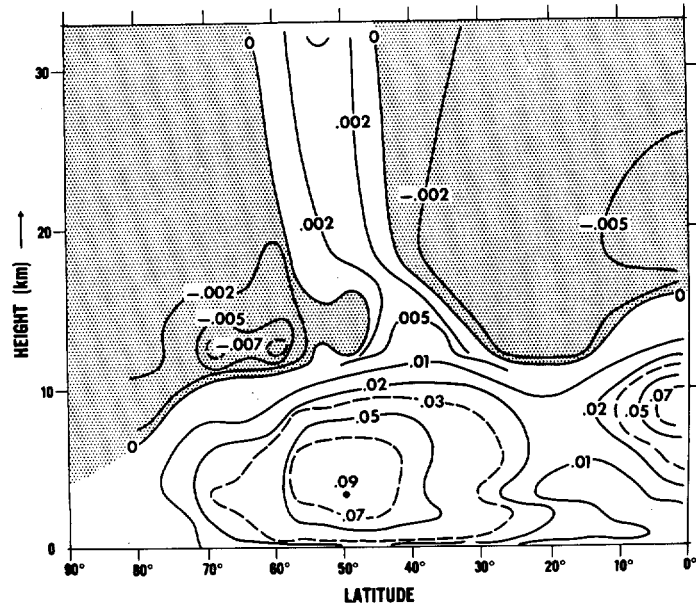


FIGURE 51.—Latitude-height distribution of the eddy conversion of potential energy due to transient eddies (average of two hemispheric values); units, joules cm^{-2} mb^{-1} day^{-1} .

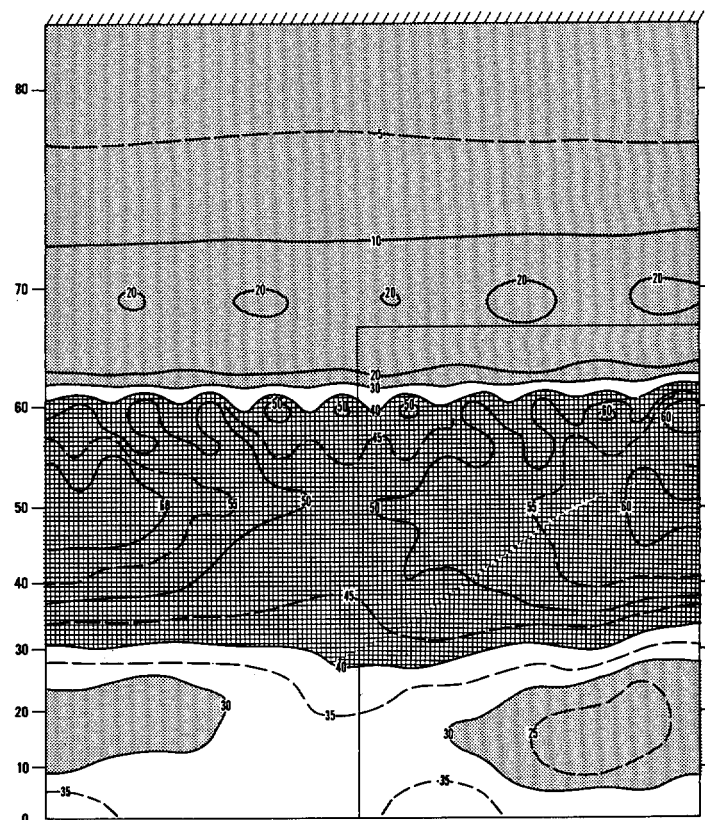


FIGURE 52.—Horizontal distribution of the vertical integral of eddy kinetic energy in the model atmosphere (average of two hemispheric values); units, joules cm^{-2} .

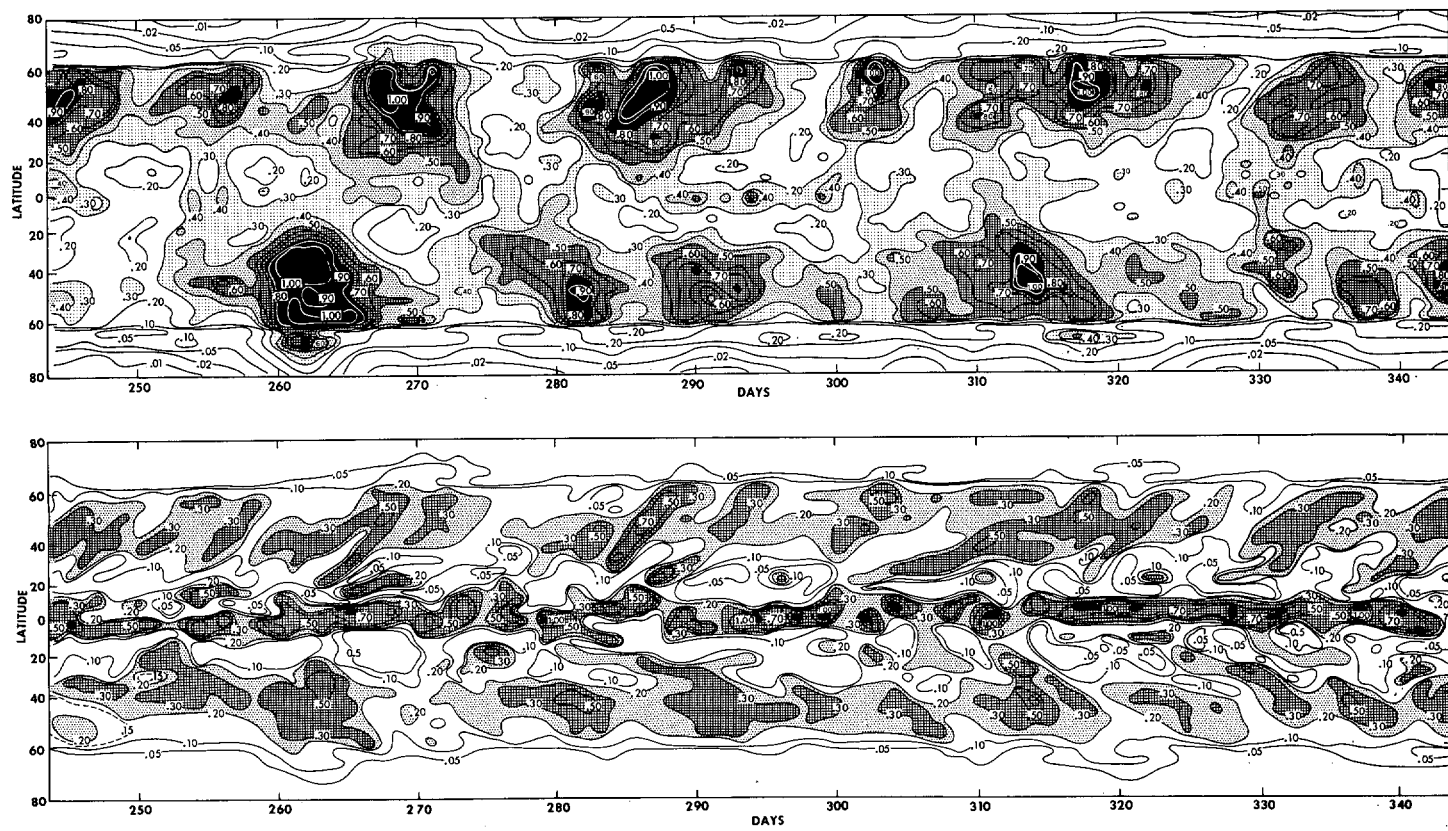


FIGURE 53.—Time isopleths of the latitudinal distribution of the vertical integral of the zonal mean eddy kinetic energy (units for the top diagram, 100 joules cm^{-2}), and of the zonal mean rate of precipitation (units for the bottom diagram, cm day^{-1}).

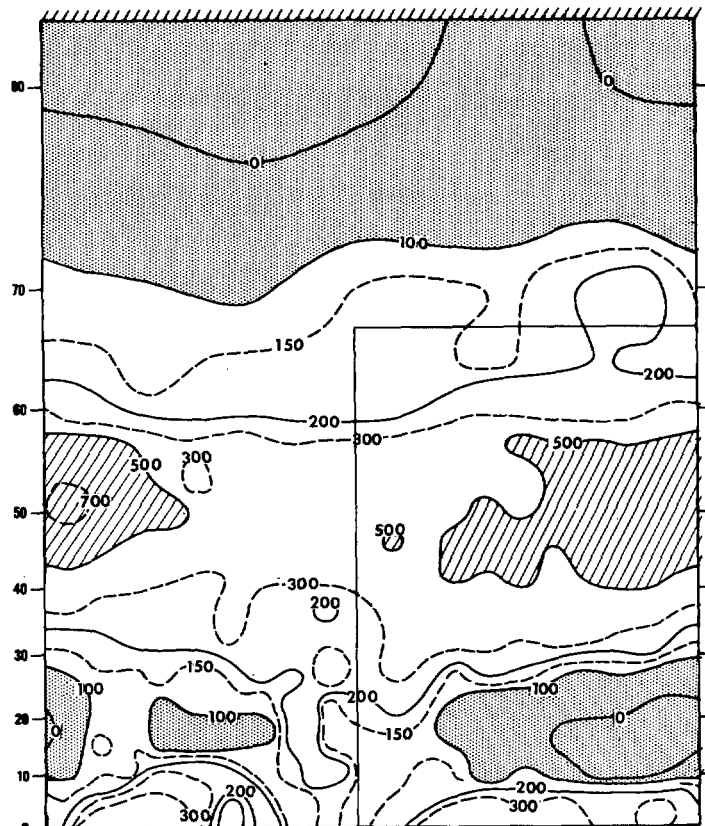


FIGURE 54.—Horizontal distribution of the conversion of available potential energy into kinetic energy due to transient eddies, that

is, $(\omega - \bar{\omega}^t)(\alpha - \bar{\alpha}^t)$. () denotes the time mean quantity, and ω and α denote vertical P -velocity and specific volume; units, 10^{-1} joules cm^{-2} day^{-1} .

The frequency distribution of cyclogenesis in the actual atmosphere, compiled by Petterssen (1950), is shown in figure 55B for comparison. Though the area of maximum frequency is located to the east of the Rocky Mountains, a secondary maximum is evident along the east coast of North America. It is noteworthy that cyclogenesis is very infrequent off the west coast of continents (for example, off the coast of northern Africa), in agreement with the result of the model experiment.

9. SUMMARY AND FUTURE STUDY

The effect of surface hydrology has been incorporated into the general circulation model developed at the Geophysical Fluid Dynamics Laboratory.

Despite the drastic idealization of land-sea configuration, general qualitative features of water and heat balance of the earth's surface are successfully simulated by the numerical time integration of this model. The interaction between the hydrology of the earth's surface and the general circulation of the model atmosphere results in a highly realistic distribution of precipitation, evaporation, and sensible heat flux and net radiative flux at the earth's surface. For example, the rain belt is maintained in the Tropics, a typical desert is formed in the subtropical region of the continent, and the subtropical belt of meager rainfall is interrupted by the relatively rainy region along the east coast of the continent.

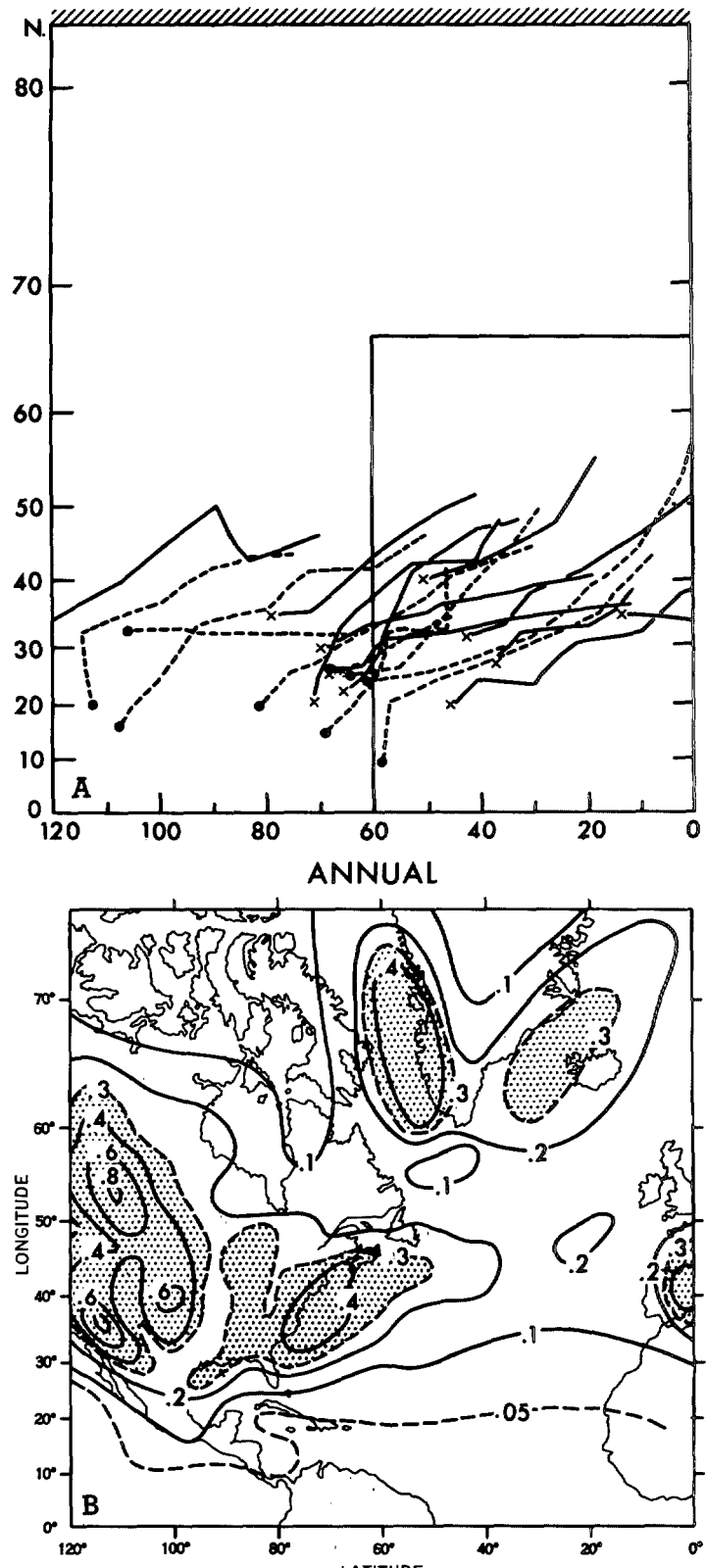


FIGURE 55.—(A) tracks of cyclones, generated in the latitude belt of 40° N. to 40° S. during 100 model days (243-343); solid and dashed lines indicate tracks in the Northern Hemisphere and Southern Hemisphere, respectively; (B) frequency of cyclogenesis, obtained by taking the average of summer and winter distributions compiled by Petterssen (1950).

In high latitudes, extensive snow cover with large albedo develops, and a situation that could correspond to the ice age emerges. The lack of seasonal variation of snow cover and the self-amplification effect of the surface

temperature upon snow cover is partly responsible for this result. In part II which follows, the effect of a poleward transport of heat by ocean circulation is incorporated in the model.

APPENDIX

Critical remarks about the choice of computational space mesh—As we described in section 2, the map distance between the finite-difference grid points on the Mercator projection map is doubled at 62.0° latitude and is quadrupled poleward of 71.8° latitude. Otherwise, it would have been necessary to choose a very short time interval for the numerical time integration because the magnification factor of the Mercator projection increases with increasing latitude.

Unfortunately, this abrupt change of grid size causes the following difficulties.

1) A so-called "computational mode" appears in the distribution of various quantities such as wind field, vertical P -velocity, surface pressure, and the rate of precipitation. In other words, abrupt doubling or halving of resolution at certain latitudes results in the alternation of large and small values from one grid point to another along the latitude circle of the abrupt change.

2) The abrupt change of resolution causes an abrupt change in magnitude of various quantities, such as in the eddy kinetic energy and in the conversion of potential energy into kinetic energy by large-scale eddies.

3) It also produces a local meridional circulation cell at the latitude of the change in resolution.

The first of these difficulties is evident in figure 52, which shows the areal distribution of the vertical mass integral of eddy kinetic energy. Along the latitude circle of the resolution change, large and small values of eddy kinetic energy alternate with each other and indicate the existence of a so-called "computational mode." A similar pattern is evident in figure 20 showing the areal distribution of the rate of precipitation. Since the computational mode is very large for the vertical P -velocity, it was necessary to average the values of two neighboring points along the latitude circle of the abrupt change in resolution in order to obtain a smooth and consistent distribution of vertical P -velocity. Figure 32, showing the areal distribution of vertical P -velocity (vertical mean value), was obtained after performing such a smoothing.

Another notable feature of figure 52 is the abrupt decrease of eddy kinetic energy from the side of higher resolution to the side of lower resolution. This is the second difficulty mentioned above.

The third difficulty is evident in figure 11A, which shows the latitude-height distribution of zonal mean vertical P -velocity. According to this figure, an intense local meridional circulation cell is located at 62° latitude where the resolution changes abruptly.

In order to eliminate these difficulties, it is necessary to change the resolution gradually. Such a scheme has already been proposed and tested by Kurihara (1965) and Kurihara and Holloway (1967).

REFERENCES

- Alpatov, A. M., "Vlagooborot kul'turnykh rastenii," (Moisture Exchange in Crops), *Gidrometeoizdat*, Leningrad, 1954, 247 pp.
- Arakawa, A., "Computational Design for Long-Term Numerical Integration of the Equations of Fluid Motion: Part I, Two-Dimensional Incompressible Flow," *Journal of Computational Physics*, Vol. 1, No. 1, July 1966, pp. 119-143.
- Batten, E. S., "A Model of the Seasonal and Latitudinal Variation of Zonal Winds and Temperatures in the Stratosphere Above 30 Km," *Memorandum RM-4144-PR*, The Rand Corporation, Santa Monica, Calif., June 1964, 28 pp.
- Berliand, T. G., "On the Change in Moisture Content of Soil and in the Heat Balance During Drought Years," *Study of the Central Geophysical Observatory*, No. 29(91), Glavnaya Geofizicheskaya Observatoriia, Trudy, Leningrad, 1952, pp. 85-96.
- Bryan, K., "A Scheme for Numerical Integration of the Equations of Motion on an Irregular Grid Free of Nonlinear Instability," *Monthly Weather Review*, Vol. 94, No. 1, Jan. 1966, pp. 39-40.
- Bryan, K., "Climate and the Ocean Circulation: III. The Ocean Model," *Monthly Weather Review*, Vol. 97, No. 11, Nov. 1969, pp. 806-827.
- Bryan, K., and Cox, M., "A Numerical Investigation of the Oceanic General Circulation," *Tellus*, Vol. 19, No. 1, Feb. 1967, pp. 54-80.
- Buch, H. S., "Hemispheric Wind Conditions During the Year 1950," *General Circulation Project, Final Report*, Part 2, Contract No. AF19-122-153, Department of Meteorology, Massachusetts Institute of Technology, Cambridge, 1954, 126 pp.
- Budyko, M. I., "Teplov δ balans zemnoi poverkhnosti," (Heat Balance of the Earth's Surface), *Gidrometeoizdat*, Leningrad, 1956, 255 pp.
- Budyko, M. I. (Editor), *Atlas Teplovo Balansa Zemnogo Shara* (Guide to the Atlas of the Heat Balance of the Earth), *Gidrometeoizdat*, Moscow, 1963, 69 pp.
- Free, G. R., Browning, G. M., and Musgrave, G. W., "Relative Infiltration and Related Physical Characteristics of Certain Soil," *Technical Bulletin No. 729*, U.S. Department of Agriculture, Washington, D.C., 1940, 52 pp.
- Gerdel, R. W., "The Transmission of Water Through Snow," *Transactions of the American Geophysical Union*, Vol. 35, No. 3, June 1954, pp. 475-485.
- Hering, W. S., and Borden, T. R., Jr., "Mean Distribution of Ozone Density Over North America, 1963-1964," *Environmental Research Papers No. 162*, U.S. Air Force Cambridge Research Laboratories, Hanscom Field, Mass., Dec. 1965, 19 pp.
- Houghton, H. G., "On the Annual Heat Balance of the Northern Hemisphere," *Journal of Meteorology*, Vol. 11, No. 1, Jan. 1954, pp. 1-9.
- Hunt, B. G., and Manabe, S., "Experiments With a Stratospheric General Circulation Model: II. Large-Scale Diffusion of Tracers in the Stratosphere," *Monthly Weather Review*, Vol. 96, No. 8, Aug. 1968, pp. 503-539.
- Jacobs, W. C., "The Energy Exchange Between the Sea and Atmosphere and Some of Its Consequences," *Bulletin of the Scripps Institution of Oceanography*, Vol. 6, No. 2, 1951, 122 pp.
- Kurihara, Y., "Numerical Integration of the Primitive Equations on a Spherical Grid," *Monthly Weather Review*, Vol. 93, No. 7, July 1965, pp. 399-415.
- Kurihara, Y., and Holloway, J. L., Jr., "Numerical Integration of a Nine-Level Global Primitive Equations Model Formulated by the Box Method," *Monthly Weather Review*, Vol. 95, No. 8, Aug. 1967, pp. 509-530.
- London, J., "A Study of the Atmospheric Heat Balance," *Final Report*, Contract No. AF19(122)-165, Department of Meteorology and Oceanography, New York University, July 1957, 99 pp.
- London, J., "Mesospheric Dynamics: Part III. The Distribution of Total Ozone in the Northern Hemisphere," *Final Report*, Contract No. AF19(604)-5492, Department of Meteorology and Oceanography, New York University, May 1962, pp. 68-108.

- Lvovitch, M. I., and Ovtchinnikov, S. P., "River Drainage," *Physical-Geographical Atlas of the World*, Akademy of Science SSSR and Central Administration of Geodesy and Cartography of USSR, Moscow, 1964, 298 pp. (see pp. 60-61).
- Manabe, S., "Climate and the Ocean Circulation: II. The Atmospheric Circulation and the Effect of Heat Transfer by Ocean Currents," *Monthly Weather Review*, Vol. 97, No. 11, Nov. 1969, pp. 775-805.
- Manabe, S., and Hunt, B. G., "Experiments With a Stratospheric General Circulation Model: I. Radiative and Dynamic Aspects," *Monthly Weather Review*, Vol. 96, No. 8, Aug. 1968, pp. 477-502.
- Manabe, S., and Möller, F., "On the Radiative Equilibrium and Heat Balance of the Atmosphere," *Monthly Weather Review*, Vol. 89, No. 12, Dec. 1961, pp. 503-532.
- Manabe, S., and Smagorinsky, J., "Simulated Climatology of a General Circulation Model With a Hydrologic Cycle: II. Analysis of the Tropical Atmosphere," *Monthly Weather Review*, Vol. 95, No. 4, Apr. 1967, pp. 155-169.
- Manabe, S., Smagorinsky, J., and Strickler, R. F., "Simulated Climatology of a General Circulation Model With a Hydrologic Cycle," *Monthly Weather Review*, Vol. 93, No. 12, Dec. 1965, pp. 769-798.
- Manabe, S., and Strickler, R. F., "On the Thermal Equilibrium of the Atmosphere With Convective Adjustment," *Journal of the Atmospheric Sciences*, Vol. 21, No. 4, July 1964, pp. 361-385.
- Manabe, S., and Wetherald, R. T., "Thermal Equilibrium of the Atmosphere With a Given Distribution of Relative Humidity," *Journal of the Atmospheric Sciences*, Vol. 24, No. 3, May 1967, pp. 241-259.
- Mastenbrook, H. J., "Frost-Point Hygrometer Measurements in the Stratosphere and the Problem of Moisture Contamination," *Humidity and Moisture—Measurement and Control in Science and Industry*, Vol. 2, Reinhold Publishing Corporation, New York, 1965, pp. 480-485.
- Murgatroyd, R. J., "Some Recent Measurements by Aircraft of Humidity up to 50,000 Ft. in the Tropics and Their Relationship to the Meridional Circulation," *Symposium on Atmospheric Ozone, Oxford, 20-25 July 1959*, Monograph No. 3, International Geodetic and Geophysical Union, Paris, Jan. 1960, p. 30.
- Oort, A. H., "On the Energetics of the Mean and Eddy Circulation in the Lower Stratosphere," *Tellus*, Vol. 16, No. 4, Nov. 1964, pp. 309-327.
- Palmer, C. C., Environmental Data Service, ESSA, Washington, D.C., 1966 (private communication).
- Peixoto, J. P., "Hemispheric Humidity Conditions During the Year 1950," *Scientific Report* No. 3, Contract No. AF19(604)-2242, Department of Meteorology, Massachusetts Institute of Technology, Cambridge, Oct. 1958, 25 pp.
- Peixoto, J. P., "Hemispheric Temperature Conditions During the Year 1950," *Scientific Report* No. 4, Contract No. AF19(604)-6108, Department of Meteorology, Massachusetts Institute of Technology, Cambridge, Nov. 1960, 211 pp.
- Peixoto, J. P., and Crisi, A. R., "Hemispheric Humidity Conditions During the IGY," *Scientific Report* No. 6, Contract No. AF19(628)-2408, Department of Meteorology, Massachusetts Institute of Technology, Cambridge, Nov. 1965, 166 pp.
- Petterssen, S., "Some Aspects of the General Circulation of the Atmosphere," *Centenary Proceedings of the Royal Meteorological Society*, 1950, pp. 120-155.
- Philip, J. R., and de Vries, D. A., "Moisture Movement in Porous Materials Under Temperature Gradient," *Transactions of the American Geophysical Union*, Vol. 38, No. 2, Apr. 1957, pp. 222-232.
- Priestley, C. H. B., "A Survey of the Stress Between the Ocean and the Atmosphere," *Australian Journal of Scientific Research*, Ser. A., Vol. 4, No. 3, Sept. 1951, pp. 315-328.
- Rasmusson, E. M., and Oort, A. H., "Mean Monthly General Saturation North of 10° S.: I. Mean Values of Meteorological Parameters," *ESSA Technical Report*, U.S. Department of Commerce, Denver, Colo., 1970 (to be published).
- Romanova, E. N., "The Influence of Forest Belts on the Vertical Structure of Wind and on the Turbulent Exchange," *Study of the Central Geophysical Observatory*, No. 44(106), Glavnaya Geofizicheskaya Observatoriia, Trudy, Leningrad 1954, pp. 80-90.
- Smagorinsky, J., Manabe, S., and Holloway, J. L., Jr., "Numerical Results From a Nine-Level General Circulation Model of the Atmosphere," *Monthly Weather Review*, Vol. 93, No. 12, Dec. 1965, pp. 727-768.
- Starr, V., and White, R. M., "Balance Requirements of the General Circulation," *Studies of the Atmospheric General Circulation, Final Report*, Part I, Contract No. AF19(122)-153, Department of Meteorology, Massachusetts Institute of Technology, Cambridge, May 31, 1954, pp. 186-242.
- Sverdrup, H. U., Johnson, M. W., and Fleming, R. H., *The Oceans, Their Physics, Chemistry, and General Biology*, Prentice-Hall Inc., New York, 1942, 1,087 pp.
- Szava-Kovats, J., "Verteilung der Luftfeuchtigkeit auf die Erde," (Distribution of the Humidity of the Air Over the Earth), *Annalen der Hydrographie und Maritimen Meteorologie*, Vol. 66, No. 8, Ernest Siegfried Mittler & Sohn, Berlin, 1938, pp. 373-378.
- Telegadas, K., and London, J., "A Physical Model of the Northern Hemisphere Troposphere for Winter and Summer," *Scientific Report* No. 1, Contract No. AF19(122)-165, Research Division, College of Engineering, New York University, Feb. 1954, 55 pp.
- Tucker, G. B., "Zonal Winds Over the Equator," *Quarterly Journal of the Royal Meteorological Society*, Vol. 90, No. 386, Oct. 1964, pp. 405-423.
- U.S. Department of Agriculture, *Year Book of Agriculture*, Washington, D.C., 1955, 751 pp. (see pp. 120-137).
- U.S. Weather Bureau, *Normal Weather Maps, Northern Hemisphere Sea Level Pressure*, Washington, D.C., 1946, 1 p. plus 13 charts.
- Wallace, J. M., "On the Role of Mean Meridional Motions in the Biennial Wind Oscillation," *Quarterly Journal of the Royal Meteorological Society*, Vol. 93, No. 396, Apr. 1967, pp. 176-185.

[Received February 3, 1969; revised June 9, 1969]